CHALMERS

# A study of three iron-based oxygen carriers in a Chemical Looping Combustion process with a Victorian brown coal

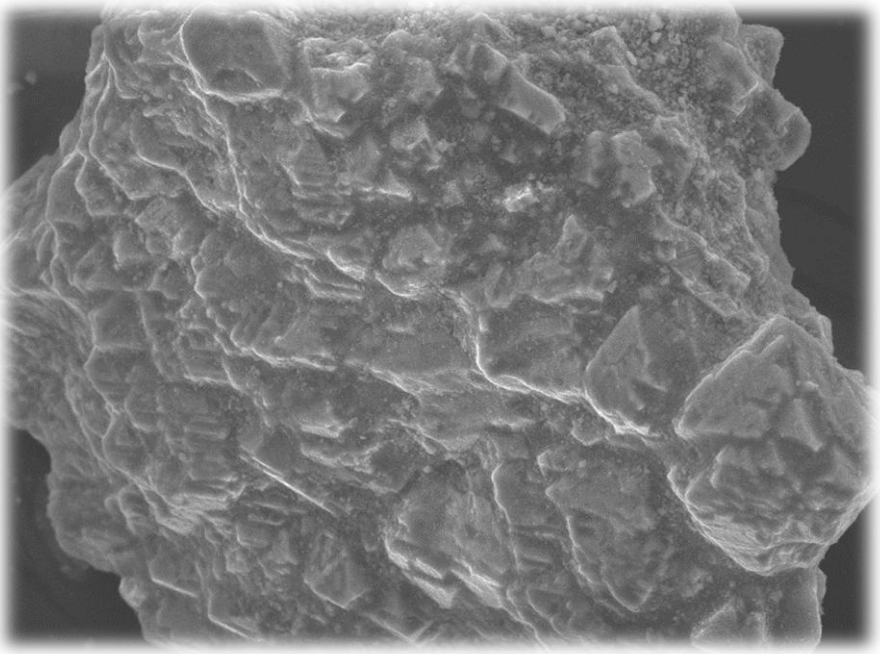

*Master of Science Thesis in Master program Innovative and sustainable chemical engineering, MPISC*

**Tove Karlsson**

Department of Chemical and Biological Engineering
*Division of Energy and Materials*
CHALMERS UNIVERSITY OF TECHNOLOGY
412 96 Gothenburg, Sweden, 2014
This work was performed at the Department of Chemical Engineering at Monash University, Australia

# A study of three iron-based oxygen carriers in a Chemical Looping Combustion process with a Victorian brown coal

**TOVE KARLSSON**

Supervisors: Professor Sankar Bhattacharya and Mr Sharmen Rajendran
Department of Chemical Engineering, Monash University, Australia

Examiner: Associate Professor Henrik Leion
Chemical and Biological Engineering, Environmental Inorganic Chemistr

Department of Chemical & Biological Engineering
CHALMERS UNIVERSITY OF TECHNOLOGY
Göteborg, Sweden 2014

# A study of three iron-based oxygen carriers in a Chemical Looping Combustion process with a Victorian brown coal

TOVE KARLSSON



Department of Chemical & Biological Engineering
Chalmers University of Technology
SE-412 96 Göteborg
Sweden

This work was performed at the Department of Chemical Engineering at Monash University, Australia, 20th of January to the 30th of May 2014.

Cover:
A SEM picture of a fresh WA-1 particle at a magnification of 500x

Division of Energy and Materials
Göteborg, Sweden 2014

# ACKNOWLEDGEMENT

The author acknowledges the support of Monash University and the Chemical Engineering department for their hospitality and help for this Master thesis project. A thanks to ÅForsk and Fredrika-Bremer-Förbundets stipendiestiftelse (Fredrika Bremer Association Scholarship Foundation) for making the collaboration between Chalmers University of technology, Sweden and Monash University, Australia possible.

# ABSTRACT

It is generally accepted that the rising global temperature is due to the increasing concentration of greenhouse gases in the atmosphere, where the majority of the global greenhouse gases emission is derived from energy production [1]. Coal is extensively used all over the world to meet the local energy needs due to its wide availability and low cost. If coal is to continue to serve as a primary energy source new technologies with higher efficiency or methods of less energy intensive capture of carbon dioxide is needed [2]. One method is Chemical Looping Combustion (CLC). In CLC, a metal oxide is used to transport oxygen for oxidation of the fuel, and is termed oxygen carrier (OC).

This study consisted of two parts involving both experimental and modelling aspects. The modelling part in this study is a preliminary model aimed at simulating the operation of a $10kW_{th}$ fluidized bed reactor system. In the experimental part, Limonite and two iron ores from Western Australia, denoted as WA-1 and WA-2, were used together with a Victorian brown coal. The oxygen carriers were evaluated through Temperature Programed Reduction (TPR), Temperature Programed Oxidation (TPO), Thermogravimetric Analysis (TGA) and in a Fluidized bed reactor (FB). The fresh oxygen carrier, TGA sample residues and FB residues were characterised with Scanning Electron Microscopy (SEM), Energy Dispersive X-Ray Spectroscopy (EDX) and X-Ray Diffraction (XRD). The fresh oxygen carrier and FB residues were also evaluated with Accelerated Surface Area and Porosimetry (ASAP).

Based on the results from the TPR/TPO and TGA experiment, the capacity of WA-1 was found to be the largest on account of its high $Fe_2O_3$ content. The three iron ores showed a stable cyclic behaviour when evaluated for 5 cycles and full conversion of coal was evident from the TGA experiments. Limonite showed the best redox reactivity compared to the other oxygen carriers even though it contained the least amount of $Fe_2O_3$. The WA-1 and WA-2 samples showed a conversion of around 40%, when Limonite had values around 80% after 10 cycles in a fluidized bed reactor (FB). The OCs appeared to lose their reactivity in the first few cycles, but after 10 cycles showed a stable behaviour. The reduced OCs after the $10^{th}$ cycle showed the presence of both $Fe_2O_3$ and $Fe_3O_4$. There was no agglomeration in any of the experiments. The coal used in this study shows promising results for a future CLC process in terms of conversion. The results from the experiments showed that Limonite was the best OC for a future CLC process using the coal tested. Porosity and the content of other minerals in the ore are the factors for its good reactivity.

The process model developed using Aspen Plus were based on two types of reactors with the first being RGibbs reactor operating on the principal of minimization of Gibbs free energy. The second one was RBatch reactor using a number of different kinetic parameters. The results showed that $Fe_2O_3$ is a good starting point for a CLC unit as an oxygen carrier for use with the Victorian brown coal. An almost complete conversion in the fuel reactor and total conversion in the air reactor was obtained for the models based on the Gibbs reactors. A number of kinetic parameters were studied in the model with batch reactors, giving a wide range of results. The air reactor showed rate dependence to the inflow of $O_2$ into the reactor. Further development of kinetics and also comparison between experimental and model predictions needs to be done.

# TABLE OF CONTENTS

# 1. INTRODUCTION

Changes in the earth´s climate have been a frequently discussed subject over the past few decades. It is generally accepted that the rising mean global temperature is due to the increasing concentration of greenhouse gases in the atmosphere. A significant rise in temperature can cause drastic changes in nature such as rising ocean levels, extreme weather fluctuations and melting of glaciers [3]. Around 65 % of the global greenhouse gas ( $CO_2$, $NO_x$, $SO_x$, $CH_4$) emission is derived from energy production [1], with the most prevalent gas being carbon dioxide [3, 4].

Today's society uses large amounts of energy, and it is therefore important to find ways to generate energy without releasing enormous amounts of carbon dioxide into the atmosphere. Coal is extensively used all over the globe to meet our energy needs due to its wide availability and low cost. However, new technologies with higher efficiency and methods of more energy efficient capture of carbon dioxide are needed if coal is to continue to serve as a primary energy source [2].

## 1.1 Background

Carbon dioxide Capture and Storage (CCS) is a process aimed at capturing carbon dioxide from power generation facilities which produce vast amounts of $CO_2$ and store it, preventing its release into the atmosphere. The gas can be stored in different locations such as under the ocean, deep saline formation, coal seams as well as depleted oil and gas reservoirs [2]. The various storage possibilities and separation process are currently under development. The Statoil Company has sequestered 14 million tons of $CO_2$ between 1996 to the beginning of 2013 into the North Sea [5] with no evidence of leakage [6]. There are two ways that have been proposed to sequester $CO_2$ into the sea. The first way is to pump the $CO_2$ to a depth of 1500m, where the $CO_2$ and seawater solution would have a higher density than seawater and would sink. The second way is to release $CO_2$ at a depth of 3000 meters where it would form liquid $CO_2$ due to the high pressure, creating a $CO_2$ lake. More studies needs to be done to predict the future $CO_2$ storage capacity. Studies about the environmental impact on marine life [4] is also a necessity before such a location is used as a $CO_2$ reservoir.

There are three main categories for carbon dioxide separation: Pre-combustion capture, Post-combustion capture and Oxyfuel combustion [2, 4].

Pre-combustion is a process whereby the fuel is gasified to syngas and reacted with water to produce carbon dioxide and hydrogen gas. The hydrogen gas can be used as a fuel in the industry or used elsewhere. This method is close to commercial deployment [2, 7].

Post-combustion is the capture of carbon dioxide after combustion through separation processes. Carbon dioxide is often separated by absorption processes with the most commonly used absorbent being Monoethanolamine (MEA) [7]. The problem with MEA is the energy intensive solvent regeneration process and that the solvent is corrosive in presence of $O_2$ [4].

Post combustion capture is expensive and incurs large energy penalties, but is presently being used for carbon dioxide separation in industrial and commercial processes [7].

Oxyfuel combustion is a technique where the fuel is burned with a gas mixture that does not contain any nitrogen gas. Often the gases are carbon dioxide and oxygen [7]. Promising results have been seen in Australia, but the technique still requires more research before it can be used in an industrial scale [4].

### 1.1.1 Chemical Looping Combustion

The methods for $CO_2$ separation mention above are expensive due to need of some sort of gas separation. An alternative CCS technology that is in a developing stage is Chemical Looping Combustion (CLC). A typical CLC reactor configuration consists of dual circulating fluidized beds termed Air Reactor (AR) and Fuel Reactor (FR). CLC uses oxygen carriers (OC), which are typically metal oxides, to transport oxygen to the FR where the metal oxide is reduced by the fuel which gets oxidized in the process. Fuel used in CLC is usually either in a solid or gaseous state, with limited studies using liquid fuels [8]. Gaseous fuel has been studied to a greater depth compared to solid fuels. The fuel type causes differences in reactor configuration and in what type of oxygen carriers to use. [9]. Solid fuels can be found in a larger quantity than natural gas, and it is often less expensive, which makes it an attractive fuel for CLC [10]. Chemical looping is aimed at generating a highly pure $CO_2$ stream for possible sequestration, but it can also be used to produce hydrogen. [9].

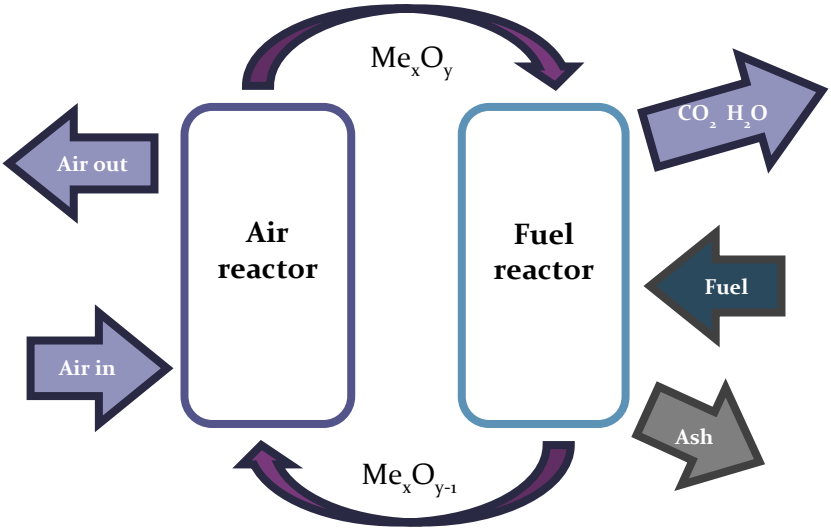


**Figure 1. Representation of a CLC process**

Figure 1 shows a schematic of the CLC process. Oxygen carriers transport oxygen to a FR where the metal oxide is reduced, and the fuel is oxidized. The oxygen carrier is then oxidized with air in the AR and can thereafter be used again [11]. The reactions taking place in the FR are the devolatilization and gasification of the coal which leads to the generation of volatiles, $H_2$, CO and ash which are shown in Equations (1-3) [11, 12]. To obtain high conversion of the fuel, good contact between the fuel and the oxygen carriers is needed [13] which is why typically a fluidized bed reactor is employed for both reactors.

$$Coal(s) \rightarrow H_2O(g) + volatiles\ (g) + Char\ (s) \quad (1)$$

$$Char(s) + H_2O(g) \rightarrow H_2(g) + CO(g) + ash(s) \quad (2)$$

$$Char(s) + CO_2(g) \rightarrow 2CO(g) + ash(s) \quad (3)$$

Upon introduction of the oxygen carriers in the reactor, the reduction of the particles occur according to Equations (4-6) [11]. The reduction reaction is often endothermic and the oxidation reaction is exothermic. A point to note is that the total heat produced in both the reactors is the same as in conventional combustion with air [14].

$$CH_4(g) + 4Me_xO_y \rightarrow CO_2(g) + 2H_2O(g) + 4Me_xO_{y-1} \quad (4)$$

$$CO(g) + Me_xO_y \rightarrow CO_2(g) + Me_xO_{y-1} \quad (5)$$

$$H_2(g) + Me_xO_y \rightarrow H_2O(g) + Me_xO_{y-1} \quad (6)$$

During combustion, a possible side reaction termed Water Gas Shift Reaction can occur according to Equation (7) below [11].

$$H_2O(g) + CO(g) \rightarrow H_2(g) + CO_2(g) \quad (7)$$

In theory, the reaction in the air reactor is supposed to be only with the reduced oxygen carriers as shown in Equation (8). If there is some char that bypasses into the AR, then the char will burn in the reactor as shown in Equation (9) resulting in a loss of carbon dioxide capture efficiency [11]. Due to the fact that combustion is done in absence of air, the production of $NO_x$ is almost nonexistent in a CLC process, except for the nitrogen in the fuel [15].

$$Me_xO_{y-1} + \frac{1}{2}O_2 \rightarrow Me_xO_y \quad (8)$$

$$Char(s) + O_2(g) \rightarrow CO_2(g) + ash(s) \quad (9)$$

In this report the word oxidation and reduction will be used for the oxidation and reduction of the oxygen carriers, while the oxidation of the fuel will be mentioned explicitly.

The temperature in the reactors is an important operation condition as different oxygen carriers need different temperatures to perform at its best while minimizing agglomeration and excessive sintering. The fuel also affects the CLC process, depending on its state, the configuration of the system needs to be changed to obtain a good conversion [12]. Another important factor that also affects the CLC process and the reactor configuration is the solids circulation, large circulation flows have been shown to affect the carbon capture negatively [16].

Agglomeration, fouling and corrosion of heat exchangers surfaces are important design aspects to be considered. It is important to know how the bed material and fuel interact with one another to minimize or eliminate problems in the fluidized bed and downstream equipment. Laboratory based experiments are different to large fluidized bed reactors,

especially in relation to the separations of ash particles. This will affect the properties of the bed material and the measurements obtained in a laboratory may differ relative to an industrial fluidized bed combustor [17]. The residence time in the reactor needs to be sufficient to avoid char particles from either flowing into the AR and combusting or elutriating out of the FR [18]. The fluidized bed is assumed to contain a perfect mixture of fuel and oxygen carrier, but the fuel on the surface of the bed may be preferentially gasified without coming in contact with the oxygen carrier. Detection of syngas ($H_2$ and CO) from the FR exhaust is a possibility due to the gasification products of the fuel not having sufficient time to react with the oxygen carrier. Hence, it is difficult to fully convert the fuel when the fuel has to first be gasified. There is also a possibility of segregation between small and larger particles, where smaller particles would migrate to the top of the fluidized bed [19].

Different methods have been proposed to minimize the reduction in fuel conversion due to unburned gases. One such method is oxygen polishing whereby oxygen gas is used at the exhaust of the FR to combust the unburned gases. Another method is to separate the unconverted gases and send it back again into the FR to react with the oxygen carrier. The third way is to use two FRs in a row, to increase the possibility of the reduction reactions by effectively increasing the residence time. The fourth method is to use certain oxygen carriers in a process called chemical looping with oxygen uncoupling [12]. These oxygen carriers have another reaction mechanism whereby they release the oxygen present within their matrix in the FR. The very reactive oxygen will combust the fuel, independent of its physical state. This is described in more detail in a later section.

Evaluation of large scale CLC technologies has been done and simulations show that the cost of the oxygen carriers in a CLC plant is in the same range as MEA which is used in a Post-combustion capture plant, if the OCs lifetime is in the range of 300 hours [11]. The quantity of bed material in a CLC process should be minimized as this would lead to a decrease in the capital and operating costs, in terms of the number of compressors required to supply the fluidizing gas and size of equipment.

When using solid fuels, ash will be generated compared to when gaseous fuels are used. Therefore, oxygen carriers used in a CLC process with solid fuels will have a shorter lifetime due to the loss of oxygen carriers during ash removal. The oxygen carriers used in a CLC process with solid fuel should therefore have a low cost [12].

### 1.1.2 Coal

About 30 % of the total global energy is produced using coal which is typically employed for electricity generation. The largest coal producers around the world are: China, USA, India, Australia, Indonesia and Russia. The global energy consumption is expected to increase by 50 % between 2010 and 2035, with 75 % of this increase ascribed to China’s increase in energy consumption [20].

Coal has different ranks with the major ranks in ascending order being: lignite (also called brown coal), subbituminous coal, bituminous coal and anthracite, which has the highest rank. The rank of the coal is decided based on the amount of fixed carbon, moisture and volatile matter. Normally a higher rank translates to older coal that has been buried deeper in the

ground and therefore has experienced higher pressure and temperature resulting in a higher amount of fixed carbon. Lignite is usually soft, friable and can ignite spontaneously under certain conditions while anthracite is hard and needs temperature above 925 C to ignite [21].

Coal mined from different seams will contain different amounts of hydrocarbons, aromatic compounds and minerals [21]. Coals can be mined from underground mines or from surface mines depending on its location. The carbon and hydrogen content changes with different types of coal, hence different coals will have different heating values and composition. The possible interaction between the oxygen carriers and minerals present in coals in a CLC process is highly variable. This depends on the oxygen carrier used as well as the ash formed from thermal processing of the minerals present in a given coal. Some oxygen carriers are more susceptible to interaction with certain minerals and this has to be taken into account when selecting the type of oxygen carrier for a given coal.

The amount of oxygen carrier to be used needs to be sufficient to transport enough oxygen for complete combustion of the fuel. Solid-solid interactions between the fuel and oxygen carrier is not high enough to be appreciable; therefore it is necessary to gasify the fuel. Taking this into account, it has been found that gasification is the rate determining step in a CLC process[22].

Australia is one of the leading coal exporters in the world, both for generation of electricity and production of steel using coking coal. Australia is expected to continue to be a significant exporter of coal in the years to come [20]. Victoria is a state in Australia with large resources of brown coal, over 500 years of at the current rate of consumption [23]. The possibility of using CLC with different Victorian brown coals is an important step when considering low emission combustion techniques for the future of Australia's power generation.

### 1.1.3 Oxygen carriers

The choice of oxygen carriers is important as previously mentioned. The criteria for oxygen carrier selection is that it should have good reactivity, the ability to fully convert the fuel, negligible attrition and agglomeration , low cost , be environmentally benign and should not pose a health risk in its handling and use [12]. The oxygen carrier also needs to be capable of fluidization as well as maintain mechanical and chemical stability during repeated redox cycles [4]. Typically, gaseous fuels are used with highly reactive oxygen carries which are generally costly, while solid fuels are used with a low cost oxygen carriers [9].

Transitions metals such as Ni, Cu, Co, Fe, and Mn and are possible oxygen carriers. W, Mo, Nb, V, Ce, In and Sn can be reduced and oxidized but due to low melting point, some of these candidates are not suitable for a CLC process [4]. For example Co has good thermodynamics for oxidation and reduction but is expensive and coupled with potential health and safety issues makes it unsuitable as a candidate for a CLC process [9]. The oxygen carriers which have been significantly tested are the Fe-, Ni-, Cu- and Mn-based materials. There has also been research into mixing of metal oxides to improve the oxygen carriers' abilities with the added metals investigated being Ca, Fe, Si, Mg, Cu and Ni [12]. Due to the low price of Fe and Cu, these metals are attractive oxygen carriers to further investigate. The use of Cu requires a lower working temperature due to its low melting point compared to other oxygen

carriers [24]. Mixture of different metals oxides that have the capability to act as oxygen carriers have been evaluated, for example $CuFe_2O_4$ showed superior performance compared to single oxygen carrier materials [25]. Ni- based oxygen carriers have a high reactivity and superior strength compared to other oxygen carriers [4] but is more expensive than other candidates and toxic.

Natural mineral ores and industrial byproducts are also possible options for oxygen carriers [26, 27]. The mineral ilmenite is a low-cost oxygen carrier that has been evaluated in a number of studies. It contains Fe and Ti in the form of $FeTiO_3$. Leion et al. (2008) concluded that ilmenite results in high conversion of CO and moderate conversion of $CH_4$ with no tendency of deactivation after 3 days of experiments [28]. Cuadrat et al. (2012) evaluated the behaviour of ilmenite as an oxygen carrier and found that structural changes could be observed whereby the porosity of the particles increased from 1.2% to 38% after 100 reaction cycles [29]. Berguerand et al. (2008 and 2010) used ilmenite in a 10 $kW_{th}$ reactor with solid fuels with stable operation for 11h obtaining $CO_2$ capture in the range of 60 to 75%; they also found that by increasing the temperature, better results could be obtained. [13, 30]. Ilmenite has shown to be resilient to ash interaction when it was mixed with different ash minerals in a study by Keller (2014) while other oxygen carriers such as $CuO/MgAl_2O_4$ and $Mn_3O_4/ZrO_2$ were more affected by the ash minerals [31]. Another potential oxygen carrier is industrial residues such as iron scale from steel production. Leion et al. (2009) showed that it is possible to use this as an oxygen carrier and in some cases the conversion of syngas and methane was similar to manufactured $Fe_2O_3/MgAl_2O_4$ OCs [10]. Other options for oxygen carriers have been investigated such as sulphates, for example $CaSO_4$ [9]. Fan et al. (2014) showed that the bimetallic oxygen carriers, $NiFe_2O_4$, $CuFe_2O_4$ and $MnFeO_3$ showed better performance compared to pure $Fe_2O_3$ [32]. Synergistic effects have been observed between bimetallic oxygen carriers such as $CuO\text{-}Fe_2O_3$ resulting in better oxygen release capacities for CuO [33].

The most common and cheapest metal in nature is iron. It has favorable characteristics to be used as an oxygen carrier and it would be ideal to use iron ores as an oxygen carrier without having to first refine it [4]. Natural iron ore is often a mixture of hematite ($Fe_2O_3$), goethite ($\alpha$-FeO(OH)), limonite ($FeO(OH)nH_2O$) and magnetite ($Fe_3O_4$) [34]. The reduction reaction of hematite to iron is a slow process, and the favorable process is for the hematite to reduce to magnetite. Different reduction mechanisms of $Fe_2O_3$ have been proposed throughout literature [35]. Investigation showed the presence of two peaks during experiments with $H_2$ reduction of $Fe_2O_3$ [36]. The first peak represented the reduction of $Fe_2O_3$ to $Fe_3O_4$ while the second was of $Fe_3O_4$ to Fe. Similar results with two peaks during the reduction of $Fe_2O_3$ have also been shown by Li et al. (2010) [37], while another investigation did not show two peaks [38].

To improve the reaction with iron, support materials have been used which increase the surface area and physical strength of the generated oxygen carrier. $Al_2O_3$ has been proven to be a good support material for use with iron [39].Observation of the reaction of a few different ores together with methane in presence of steam gasification of coal showed that Limonite and Magnetite had better reactivity compared to the other materials evaluated in that study [40].

Chemical Looping with Oxygen Uncoupling (CLOU) is done using certain oxygen carriers that have a different reaction mechanism compared to the oxygen carriers used in CLC. Oxygen carriers suitable for CLOU need to have an equilibrium concentration of $O_2$ at the temperatures used in a FR [10]; this makes the oxygen carrier to release its oxygen in the FR and thereafter the very reactive gaseous oxygen will oxidize the solid fuel. CuO has shown good performance as an oxygen carrier for CLOU. The advantage with this method is that the rate limiting gasification reaction in a normal CLC no longer exists [10, 12].

Ruben et al. (2011) found that ash from coal was not harmful for the oxygen carriers which were investigated and that in some cases the minerals in the ash increased the oxygen carriers' reactivity. The experiments were carried out in a Thermogravimetric analyzer (TGA) and the presence of ash led to an increase in the porosity and surface area of the oxygen carrier allowing for increased access of the reducing gases to the active sites. It is unclear, however, if similar results will be observed in a fluidized bed [41].

Leion et al. (2007, 2008) used synthetic oxygen carrier particles such as $Fe_2O_3/MgAl_2O_4$ in their study. They concluded that the reactivity of the oxygen carrier is not the rate limiting step in a CLC process, but rather the gasification of the fuel. Gasification rate increases with the use of oxygen carriers due the removal (oxidation) of $H_2$ and CO gases, which are known gasification inhibitors, by the oxygen carriers. No agglomeration was found in either of the studies. The use of steam as a gasification agent in the fluidized bed significantly increased the conversion rate of the fuel in both the studies [19, 22].

The economical aspect needs to be taken into account when evaluating the oxygen carriers. Ongoing costs needs to be accounted for such as the addition of fresh oxygen carriers to replace the particles that have undergone attrition or deactivation as well as those which were lost during the ash separation step [11]. Hence, cheap oxygen carriers are preferred for this reason.

### 1.1.4 Working CLC units

There have been a number of studies using solid fuels in CLC processes in recent years. There are a number of different experimental CLC facilities ranging from 1 $kW_{th}$ up to couple of $MW_{th}$.

At Chalmers University in Sweden there are two units having capacities of 10 $kW_{th}$ and 100 $kW_{th}$. The 10 $kW_{th}$ unit has been used in several studies with different solid fuels and oxygen carriers. Berguerand et al. (2008) and Linderholm et al. (2012) are just a few examples in the literature which used the 10 $kW_{th}$ unit. Berguerand et al. (2008) result has been mention previously and Linderholm et al. (2012). showed that the gasification rate of the fuel was enhanced by using Manganese ore [13, 27]. The 100 $kW_{th}$ unit has been used by Markstrom et al. (2012, 2014) with different coals and showed a stable operation with minimal loss of char into the AR resulting in high $CO_2$ capture efficiencies [42, 43].

At Southeast University in Nanjing, China there is a 1 $kW_{th}$ unit which has been operated with iron ore as the oxygen carrier and a 10 $kW_{th}$ unit that has been used with coal and biomass as fuels with Ni- and Fe-based oxygen carriers. Shen et al. (2009) conducted a study with iron

oxide and biomass in the 10 $kW_{th}$ unit and found that the gasification of the biomass was more temperature dependent than the oxidation of the fuel by the oxygen carrier. The tests were conducted for 30 hours without changing the oxygen carrier [44].

Abad et al. (2012) used a 1.5 $kW_{th}$ unit at CSIC , Zaragoza in a CLOU mode of operation with solid fuel and obtained 100% conversion, with even a few percent of $O_2$ being found in the FR's exhaust [45].

IFP in Lyon, France has a 10 $kW_{th}$ plant having three reactors with two ARs in series. Yazdanpanah et al. (2014) made a reactor model and validated it against experimental values obtained from the 10 $kW_{th}$ unit. The model was able to predict the outlet concentrations of $H_2$ and CO as well as the $CO_2$ yield [46].

Thon et al. (2013) from Hamburg University have performed experiments using a 25 $kW_{th}$ unit with a two stage fluidized bed reactor. They have studied the use of ilmenite with solid fuels and obtained an outlet concentration of $CO_2$ of more than 90 vol % [47].

One of the largest plants is the 1$MW_{th}$ CLC plant in Dramstadt which has published operational results showing that the FR is working as expected [48] but further investigation is ongoing. Alstom Power Plant Laboratories are developing a CLC plant having a capacity of 3$MW_{th}$ and testing on the plant has begun [49].

### 1.1.5 Studies of Victorian Brown coal

There have only been a few studies with Victorian brown coal, which typically has very low ash content and a high amount of oxygen, as a fuel for CLC.

Saha et al. (2011) investigated Loy Yang, a type of Victorian brown coal with NiO and CuO oxygen carriers. They used a TGA in their study and reported 5 cycles of reduction and oxidation of the oxygen carrier in presence of coal. Two different temperatures were studied, 950 °C and 800 °C. The reason a lower temperature was used was because CuO was found to sinter at 950 °C and that the re-oxidation was hard to accomplish at this temperature. Since the ash content in Loy Yang was very low, ash separation after each cycle was not possible and it therefore accumulated in each subsequent cycle. CuO displayed high reactivity with a combustion conversion of 96% while this value was only 67% with NiO [23].

In another study by Saha et al. (2012), Loy Yang coal was investigated again and this time with $Fe_2O_3$ and NiO oxygen carriers. They found that agglomeration was not evident between $Fe_2O_3$ and Loy Yang coal's ash with no loss in the mass of the oxygen carriers used. A subsequent decrease in reactivity of the OCs was observed, with $Fe_2O_3$ and NiO showing a combustion percentage of 89% and 67% respectively in the $5^{th}$ cycle [50].

Experiments showed that the reduction reactivity of CuO and NiO with Victorian coal had its highest rate at the second cycle, and then decreased. This may be due to structural changes during the first cycle and the decrease later on due to accumulation of ash. It was found that the oxidation was not affected by the accumulation of ash [23].

In Leion et al. (2008), a few different coals were investigated of which one was an Indonesian coal similar in composition to the coal used in this study. They found that it was possible to separate the reaction of char from the reaction of volatiles for the Indonesian coal, due to its high content of volatiles compared to the other coals which were studied. The required residence time was found to be shorter for coals containing higher amounts of volatile matter [19].

A fair number of studies using coal in a CLC process have been performed but there are very few investigations which have used Victorian brown coal as a fuel for CLC. Therefore further studies are needed to identify the possible issues associated with using such a fuel in CLC.

## 1.2 Objectives

This study aims at evaluating the reactivity of three different oxygen carriers with one type of Victorian brown coal. A secondary aim of the project is the development of a preliminary Aspen Plus model, for a Victorian brown coal fuelled CLC in a fluidized bed reactor, using one of the evaluated oxygen carriers in this study.

## 1.3 Boundaries

The project aims to evaluate the performance of three oxygen carriers against one Victorian brown coal using a Thermogravimetric analyser (TGA) and a fluidized bed reactor over multiple redox cycles. The OCs will first be evaluated with a Temperature programmed reduction/oxidation (TPR/TPO) measurements without the coal. This will be done at one pressure and one temperature.

## 1.4 Issues to be examined

- Is the reactivity and capacity significantly different between the three oxygen carriers?
- Is agglomeration evident?
- Are there any interactions between the oxygen carrier and coal ash?
- Are any of these interactions detrimental to the performance of CLC of Victorian brown coal using $Fe_2O_3$-based oxygen carriers i.e. what issues are expected to arise?

# 2. MATERIALS

The Victorian brown coal which was used is Yallourn coal. The composition of the coal is shown in Table 1, Table 2 and Table 3 below. The oxygen carriers that were used are $Fe_2O_3$-based ores: The first ore is from Western Australia and is further denoted as WA-1. The second ore is also from Western Australia, denoted as WA-2. The third ore is Limonite (FeO (OH)* $nH_2O$) sourced from Indonesia. The composition of the different oxygen carriers can be found in Table 4 below.

**Table 1. Proximate Analysis of Yallourn coal**

| **Yallourn coal** | |
|---|---|
| Moisture, % ar | ~65 |
| Ash, % db | 1.9 - 2.4 |
| Volatile Matter, % db | 48.0 – 50.5 |
| Fixed Carbon, % db | 47.0 – 49.1 |
| | |
| HHV, MJ/kg | 24.5 – 26.1 |

**Table 2. Ultimate Analysis of Yallourn coal**

| **Yallourn coal** | |
|---|---|
| C, % db | 64.9 - 66.6 |
| H, % db | 4.0 - 4.6 |
| N, % db | 0.4 - 0.5 |
| S, % db | 0.2 – 0.3 |
| O, % db | ~22.5 |

**Table 3 Ash composition of Yallourn coal**

| Ash Composition (%) | |
|---|---|
| $SiO_2$ | 5.3 – 15.0 |
| $Al_2O_3$ | 3.0 – 5.0 |
| $Fe_2O_3$ | 34.1 – 40.4 |
| $TiO_2$ | 0.1 – 0.44 |
| $K_2O$ | 0.3 – 1.0 |
| MgO | 14.2 – 17.2 |
| $Na_2O$ | 4.8 – 6.0 |
| CaO | 6.3 – 8.3 |
| $SO_3$ | 13.7 – 17.0 |

**Table 4 Composition of WA-1, WA-2, and Limonite**

| *db%* | **WA-1** | **WA-2** | **Limonite** |
|---|---|---|---|
| **$Fe_2O_3$** | 95,2 | 91 | 80,1 |
| **$SiO_2$** | 2,2 | 4.9 | 4,9 |
| **$Al_2O_3$** | 1,1 | 2.7 | 5,5 |
| **$Na_2O$** | 1,2 | | 0.2 |
| **MgO** | 0,2 | 0.3 | 0,9 |
| **MnO** | | 1.0 | 1,8 |
| **$P_2O_5$** | 0.1 | 0.1 | 0.1 |
| **$SO_3$** | | | 0.1 |
| **TiO2** | | | 0.1 |
| **Co3O4** | | | 0.3 |
| **$Cr_2O_3$** | | | 3,9 |
| **NiO** | | | 1,9 |
| **Other** | 0.1 | | 0.3 |

The oxygen carriers were sieved to the size range of 150-350 µm while the coal was sieved to a range of 600-1000 µm. To enable the Limonite sample to be sieved, it was dried for 5 hr at 300 °C, to remove some of the moisture. One key observation is that the bulk density of Limonite was significantly less relative to both the WA-1 and WA-2 samples. A comparison between a calcined and a fresh WA-1 samples was also done, where the WA-1 sample was calcined at 900 °C for 3 hours.

# 3. METHODOLOGY

This study contains of two parts, the first involving experimental results with the other being modelling using Aspen Plus. The Aspen plus model is a model for future experiments in a $10kW_{th}$ fluidized bed reactor using the WA-1 oxygen carrier which was used in the experimental part of this study. The two parts are separated into individual sections. The following describe the methodology employed for the different instruments and analysis techniques used.

## 3.1 Temperature programmed reduction/oxidation (TPR/TPO)

The reduction and oxidation properties of the oxygen carriers were evaluated through Temperature programmed reduction/oxidation (TPR/TPO) measurements. A 50 mg sample of the oxygen carrier was placed on a small pad of glass wool housed within a quarts sample tube. Figure 2 shows the ChemiSorb 2720 unit from Micromeritics which was used for the analysis. The operating principle is through the use of a Thermal Conductivity Detector (TCD) which measures the difference in thermal conductivities of the gases exiting the sample tube against the carrier gas. The gas from the sample tube exit was passed through dry ice to ensure that no moisture entered the TCD detector. Reduction was done using a gas mixture containing 5 % $H_2$ in $N_2$ while oxidation was done in air. $N_2$ was used as a purge gas for 10 minutes between the reduction and oxidation reactions.

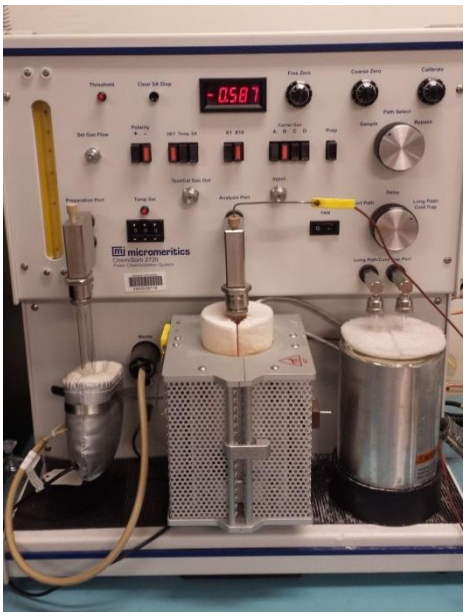


**Figure 2. TPO/TPR instrument ChemiSorb 2720**

The sample was preheated to 300 °C at a ramp rate of 20 °C /min to drive off the moisture present in the oxygen carriers. At 300 °C, the furnace was turned off and the sample was cooled to 100 °C in $N_2$ gas. Once a temperature of 100 °C was reached, the $N_2$ gas was switched to the $H_2/N_2$ gas mixture and the TCD signals that were generated was recorded. The furnace was then turned on with a ramp rate of 10 °C /min to a temperature of 900°C. When the sample temperature reached 900 °C, a dwell time of 30 min was used to ensure complete

reduction of the oxygen carrier. The temperature in the sample tube was maintained at 900 °C for the remainder of the experiment.

After the first reduction and purge, oxidation was done using air for a duration of 10 minutes. A $N_2$ purge was done at the end of the oxidation stage and before the next reduction stage to prevent the mixing of gases. The next 4 reduction reactions had a dwell time of 75 min at an isothermal temperature of 900 °C. In total, 5 redox cycles were evaluated in one experiment over a duration of 580 minutes.

## 3.2 Thermogravimetric analysis (TGA)

A Thermogravimetric analyzer (TGA) was used to study the reaction between the fresh oxygen carriers and Yallourn coal. The purpose of this experiment was to determine the OC reactivity and stability over multiple redox cycles with coal. The TGA results were displayed in terms of mass change as a function of time and temperature.

To study the effect of gasification agents, $CO_2$ and steam was used with the WA-1 sample. A comparison between the calcined and fresh WA-1 samples together with the two gasification agents were also done in the TGA.

The TGA instrument used was a NETZSCH STA 449 F3 Jupiter which can be seen in Figure 3. A steam generator from NETZSCH was also used for the experiments utilizing steam gasification.


**Figure 3. TGA used in this project**

Coal was mixed with the oxygen carriers at a 1:50 ratio for all experiments, which is higher than the stoichiometric amount required for complete combustion of the fuel by means of hematite reduction to magnetite.

500 mg of the oxygen carrier was placed in an alumina crucible and mixed with 10 mg of coal. The sample was heated at a ramp rate of 5 °C /min to 200°C and then to 900°C at a rate of

10 °C /min after which it had a 30 min dwell time in a reducing atmosphere. Oxidation was done for 30 minutes at the end of the cycle and then the sample was cooled down to room temperature to begin a new reaction cycle. 20 ml/min of $CO_2$ with 80 ml/min of $N_2$ was used for the reduction reaction and 20 ml/min of air (21 % $O_2$ and 79% $N_2$) with 80 ml/min $N_2$ was used during oxidation. The oxygen carriers where evaluated for 5 cycles, with the addition of new coal at the start of every cycle. The experiment was terminated at the end of the fifth oxidation reaction. Ash separation after each cycle was not possible due to the small amount of ash generated by the coal.

The WA-1 sample and coal mixture was also subjected to steam gasification during the reduction step in a separate experiment. The steam flow rate was 20 ml/min with 80 ml/min of $N_2$ during the reduction stage. This was done to evaluate the effect of gasification agents, similar to that which can be found in literature [19, 22].

## 3.3 Fluidized bed reactor

The last part of the experimental plan was to evaluate the oxygen carriers' performance in a fluidized bed reactor (FB). Ten reduction/oxidation (redox) cycles were performed and the change in the reactivity of the oxygen carriers was measured by means of analyzing the composition of the exhaust gases. The experiments were performed with $CO_2$ as the gasification agent.

The FB reactor was filled with 100g of the oxygen carriers and heated to 900 °C under a flow of 4.8 L/min $N_2$ and 1.2 L/min air. The gas was changed when the $O_2$ level reached a stable value signifying completely oxidized oxygen carriers. $CO_2$ was introduced at a flow rate of 1.2 L/min together with 4.8 L/min $N_2$. Once the $CO_2$ level stabilized, 1g of coal was added to the reactor. When the CO and $CO_2$ concentration returned to their initial values, the $CO_2$ flow was shut off. After the $CO_2$ level decreased to zero, air was turned on to initiate the oxidation of the oxygen carriers. The presence of a $CO_2$ peak when the air was turned on would signify incomplete combustion of char during the reduction experiment. The experiment was terminated at the end of the tenth reduction reaction.

The fluidized bed reactor is 50 mm in diameter having a height of around 1 meter. Figure 4 below shows the schematic of the setup.

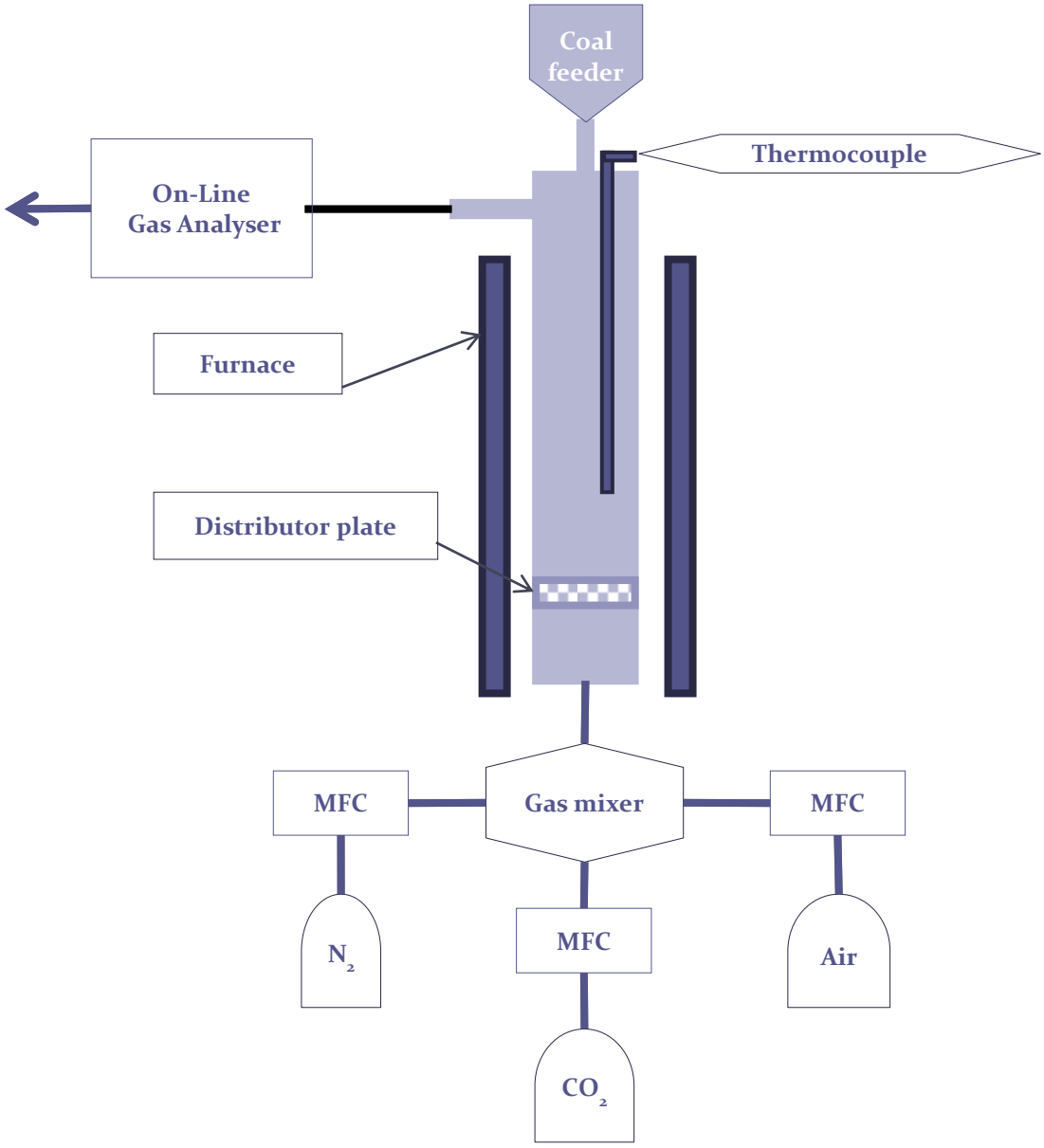


**Figure 4 Schematic setup of the fluidized bed reactor (MFC is Mass Flow controller)**

### 3.3.1 Characterization of oxygen carriers

The fresh samples alongside the residues from the TGA and the small fluidized bed reactor were evaluated with a JOEL 7001F Scanning Electron Microscope (SEM) coupled with an Oxford Instruments X-Max 80 Silicon Drift Energy Dispersive X-Ray Spectrometer (EDX) to study the changes in the morphology and surface elemental composition.

A Rigaku MiniFlex 600 X-Ray Diffractometer (XRD) was used to evaluate changes in the presence of crystalline compounds on the surface of the oxygen carrier before and after the experiment.

To obtain the Brunauer, Emmett and Teller (BET) surface area, total pore volume and the average adsorption pore diameter of the oxygen carrier particles, an Accelerated Surface Area and Porosimetry (ASAP) instrument was used. This model of the instrument was

Micromeritics ASAP 2010. Both the fresh sample and the spent particles from the fluidized bed reactor experiments were analysed using this technique.

## 3.4 Aspen Plus modeling

Four different process models for a CLC system were developed, some based on the minimization of Gibbs free energy while others were done using reaction kinetics obtained from literature. The models were developed to serve as a comparison with the experimental results from a $10kW_{th}$ fluidized bed reactor. The goal was to use the models to optimize the process parameters for the fluidized bed reactor operation.

### 3.4.1 Gibbs free energy model

A model for a CLC system was constructed in Aspen Plus. The FR was modeled with three units in which two units were needed for modeling the gasification reaction of coal and one was used for the oxidation reaction of the gas species with the oxygen carrier. Fan et al. (2008) have modeled a CLC system with 3 reaction units [51] and a similar approach was used in this model.

The reactor component RYield was used to decompose the coal into its main components. The coal components were then mixed with the fluidizing gas in a RGibbs reactor. The RGibbs reactor is an equilibrium reactor based on the minimization of Gibbs free energy. The RYeild and RGibbs units modeled the gasification reaction of coal in the FR of the CLC unit and are here named the decomposing reactor, as it represent the gasification of coal. The decomposing reactor was kept constant in all the models which were generated. Another RGibbs reactor was used for the reduction reaction wherein the oxygen carrier stream was added. This part is named as the Fuel Reactor (FR) throughout the modelling section and does not concern the gasification block. The gases coming out from the FR was separated from the solid outflow which was then sent to the AR. The gas stream was condensed to separate the liquid and gas phases. The AR was also a RGibbs reactor, where the outflow from the reactor was a mixture of oxidized oxygen carriers and oxygen depleted air which continued to a cyclone where the solids were separated.

The inflow of coal was set to 1 kg/hr with a composition as shown in Table 2 in the Materials section above. The amount of fluidizing gas for coal, termed Carbon carrier gas (CCG), was initially set to 25 L/min at 1atm and 25 °C with 20 % of $CO_2$ and balance $N_2$. The inflow of $Fe_2O_3$ was also initially set to 100 kg/hr, which is sufficient to reduce all the coal while reducing the oxygen carrier to no lower than $Fe_3O_4$. All the reactors were operated at 900 °C and 2.5 atm. The inflow of air mixture was 25 L/min consisting of 20 % of air in $N_2$, resulting in a flow of 4.2 % $O_2$ and 95.8 % $N_2$, which was sufficient to oxidize the oxygen carriers back to its highest oxidation state. Analyses were done on a few parameters including the temperature and pressure in the reactor, the CCG composition and flow rate as well as the oxygen carrier flow into the FR. Different concentrations and flow rates of $O_2$ in the air into the AR were also investigated.

### 3.4.2 A CLC model based on kinetic values

The RGibbs reactor mentioned above gives the equilibrium concentration of gases coming out from the reactor. The next model utilizes kinetics obtained from literature. By using an RBatch reactor, it was possible to add reaction kinetics to the model. The RBatch reactor was chosen due to its simplicity and it was better compared to a plug flow or CSTR reactor. Bing et al. (2012) evaluated NO and $N_2O$ formation in a fluidized bed combustor with a more sophisticated model for the FR utilizing a large amount of different kinetics [52]. The models developed in this study are much simpler than that, but could be further developed to a much more sophisticated model, when more knowledge about the system is known. The reactions used in the batch reactor are as follows:

$$CO + 3Fe_2O_3 \rightarrow CO_2 + 2Fe_3O_4 \qquad (A1)$$

$$H_2 + 3Fe_2O_3 \rightarrow H_2O + 2Fe_3O_4 \qquad (A2)$$

$$CH_4 + 12Fe_2O_3 \rightarrow 8Fe_3O_4 + CO_2 + 2H_2O \qquad (A3)$$

$$O_2 + 4Fe_3O_4 \rightarrow 6Fe_2O_3 \qquad (B1)$$

Reactions A1-A3 were used in the FR model while Reaction B1 was used in the AR. All the above reactions were used with kinetics data from Abad et al.(2007) [11, 53]. The A1 reactions were also used with reduction kinetics from Bohn et al. (2010) [54] and the oxidation reaction was similarly evaluated with kinetic from Son et al. (2006) [55] as for Abad et al. (2007).

Other kinetic models were also evaluated, with the assumption that coal gasification was the rate governing process [10, 12]. Therefore it was sufficient to represent the kinetics for the oxidation of the syngas by the oxygen carriers even if the gas species were formed in the gasification stage before. Different gasification kinetics from literature and experiments were evaluated. The reduction kinetics was only used in the fuel reactor while the air reactor was modelled as a RGibbs reactor. While evaluating the oxidation kinetics the reduction reactor was a RGibbs reactor to minimize the affect different reduction kinetics would have.

The gasification kinetics was incorporated using the Arrhenius equation, as shown below in Equation 10:

$$k = k_0 \cdot \exp\left(\frac{-E_a}{RT}\right) \qquad (10)$$

The different kinetic values used in this model can be found in Table 5. When using reaction kinetics, other possible reactions were not accounted for, so the inflow of the reactant gas was divided into two parts: the reactants for the reaction with the oxygen carrier and the "inert" part. This addition was the last and fourth model developed. The reactants were added to the batch reactor with most of the oxygen carrier. The "inert" part was directed to a RGibbs reactor containing a fraction of the oxygen carrier. This was used to evaluate if there was a change in the equilibrium composition of the other species from reactions with the oxygen carrier. Due to splitting of the streams, the composition of the streams would change resulting

in a variation of the concentration compared to the real case, but the goal here was to determine if this change was negligible and if it was possible to assume the non-reactants as inert. The different model configurations can be seen in Figure 37 to Figure 40 in the Appendix.

**Table 5. Kinetic parameters used in the Aspen Plus models**

| | **Reference** | **$k_{0\text{-}XX}$ -value ($s^{-1}$) *** | **$E_a$-activation energy (kJ/mol)** | **Conditions** |
|---|---|---|---|---|
| ***Reduction/oxidation kinetics*** | Abad et al. (2007) [11, 53] | $k_{0\text{-}A1}=9.0*10^{-4}$<br>$k_{0\text{-}A2}=2.5*10^{-4}$<br>$k_{0\text{-}A3}=8*10^{-4}$<br>$k_{0\text{-}B1}=3.1*10^{-4}$ | $E_{a\text{-}A1}=24$<br>$E_{a\text{-}A2}=20$<br>$E_{a\text{-}A3}=49$<br>$E_{a\text{-}B1}=14$ | 60% Fe support material $Al_2O_3$, (A1+A2)<br>45% Fe support material $Al_2O_3$ (A3+B1)<br>TGA-evaluation, syngas |
| ***Gasification kinetics*** - Gasification of a South Australian low-rank coal with carbon dioxide and steam: kinetics and reactivity studies | Ye et al. (1998) [56] | $k_{0\text{-}A1}=22.16667$<br>$k_{0\text{-}A2}=22.16667$ | $E_{a\text{-}A1}=91$<br>$E_{a\text{-}A2}=91$ | Bowmans coal, $CO_2$ in single-particle reactor, atmospheric pressure, temperatures 714-892°C |
| ***Gasification kinetics*** - experimental values | Rajendran (Unpublished data) | $k_{0\text{-}A1}=2.33*10^{6}$<br>$k_{0\text{-}A2}=2.33*10^{6}$ | $E_{a\text{-}A1}=212.5$<br>$E_{a\text{-}A2}=212.5$ | shrinking core model, 20% $CO_2$ in $N_2$, with $Fe_2O_3$ oxygen carrier, Yallourn coal |
| ***Gasification kinetics*** - experimental values | Tanner (Unpublished data) | $k_{0\text{-}A1}=10617.7$<br>$k_{0\text{-}A2}=10617.7$ | $E_{a\text{-}A1}=140.5$<br>$E_{a\text{-}A2}=140.5$ | TGA, 10mg Yallourn char, 90% $CO_2$ in $N_2$, shrinking core model |
| ***Gasification kinetics*** - CO2-Gasification Reactivity of Different Carbonaceous Materials at Elevated Temperatures | Gu et al. (2009) [57] | $k_{0\text{-}A1}$= 80393.6<br>$k_{0\text{-}A2}$= 80393.6 | $E_{a\text{-}A1}=174.92$<br>$E_{a\text{-}A2}=174.92$ | petroleum coke, $CO_2$ gasification TGA<br>1223 - 1673 K, |
| ***Gasification kinetics*** - Gasification kinetics of coal chars in carbon dioxide | Osafune et al. (1987) [58] | $k_{0\text{-}A1}=4600$<br>$k_{0\text{-}A2}=4600$ | $E_{a\text{-}A1}=165$<br>$E_{a\text{-}A2}=165$ | TGA, $CO_2$ gasification, 1143-1559 K, shrinking spherical<br>ash less particle model, Taiheiyo coal |
| ***Gasification kinetics*** - Gasification kinetics of coal chars in carbon dioxide | Osafune et al. (1987) [58] | $k_{0\text{-}A1}=6600$<br>$k_{0\text{-}A2}=6600$ | $E_{a\text{-}A1}=170$<br>$E_{a\text{-}A2}=170$ | TGA, $CO_2$ gasification, 1143-1559 K, shrinking spherical<br>ash less particle model, Yallourn coal |
| ***Gasification kinetics*** - $CO_2$ Gasification Kinetics of Two Alberta Coal Chars | Koviacik et al. (1991) [59] | $k_{0\text{-}A1}=2591666.67$<br>$k_{0\text{-}A2}=2591666.67$ | $E_{a\text{-}A1}=212$<br>$E_{a\text{-}A2}=212$ | Obed Mountain coal chars, TGA, Max Temp. 950°C $CO_2$ partial pressure at 0.1 Mpa, Volume reaction model. |
| ***Reduction kinetics*** | Bohnt et al. (2010) [54] | $k_{0\text{-}A1}=26695351$<br>$k_{0\text{-}A2}=26695351$ | $E_{a\text{-}A1}=75$<br>$E_{a\text{-}A2}=75$ | Reduction of $Fe_2O_3$ to $Fe3O_4$, $N_2$+CO+$CO_2$ (respectively, 82, 3 and 15 vol. %) 723 -973 K, 1 bar, A fluidized bed reactor. First order reaction |
| ***Oxidation kinetics*** | Son et al. (2006)[55] | $k_{0\text{-}B1}=0.004$ | $E_{a\text{-}B1}=6$ | A thermobalance reactor, 1223 K, $Fe_2O_3$ supported on bentonite, oxidized by 10% $O_2$, shrinking core model |
| ** Subscripts A1,A2 and A3 denotes the reactions in the FR as mentioned in the Methodology section. B1 represents the reaction in the AR,* | | | | |

# 4. RESULTS

The experimental and modelling results are presented in this section. The experimental section involves the evaluation using TPR/TPO, followed by TGA, and small fluidized bed reactor. The last part covers the different models generated using Aspen plus.

## 4.1 TPR/TPO – Capacity and Reactivity of OC

Redox experiments were conducted in the TPR/TPO unit using the three oxygen carriers. Figure 5 shows the TCD signals obtained over the five redox reactions which were performed. When the gases were changed, large negative peaks appeared which is due to the difference in the thermal conductivity of the gases relative to the carrier gas. The oxidation peak is small and often overshadowed by the peak from the changing of the gas and hence could not be separated from one another. Since the oxidation reaction is fast, it was not possible to distinguish the signals due to the change in gas and oxidation of the oxygen carrier. As mentioned in the methodology chapter, the temperature profile was increased to 900 °C, with a 10 °C/min ramp rate from 100 °C and this is clearly depicted in Figure 5. Once the set point of 900°C was reached, it was maintained throughout the rest of the experiment. There was a slight increase in temperature during each of the oxidation reactions for all the different OCs which shows that they all were exothermic reactions.

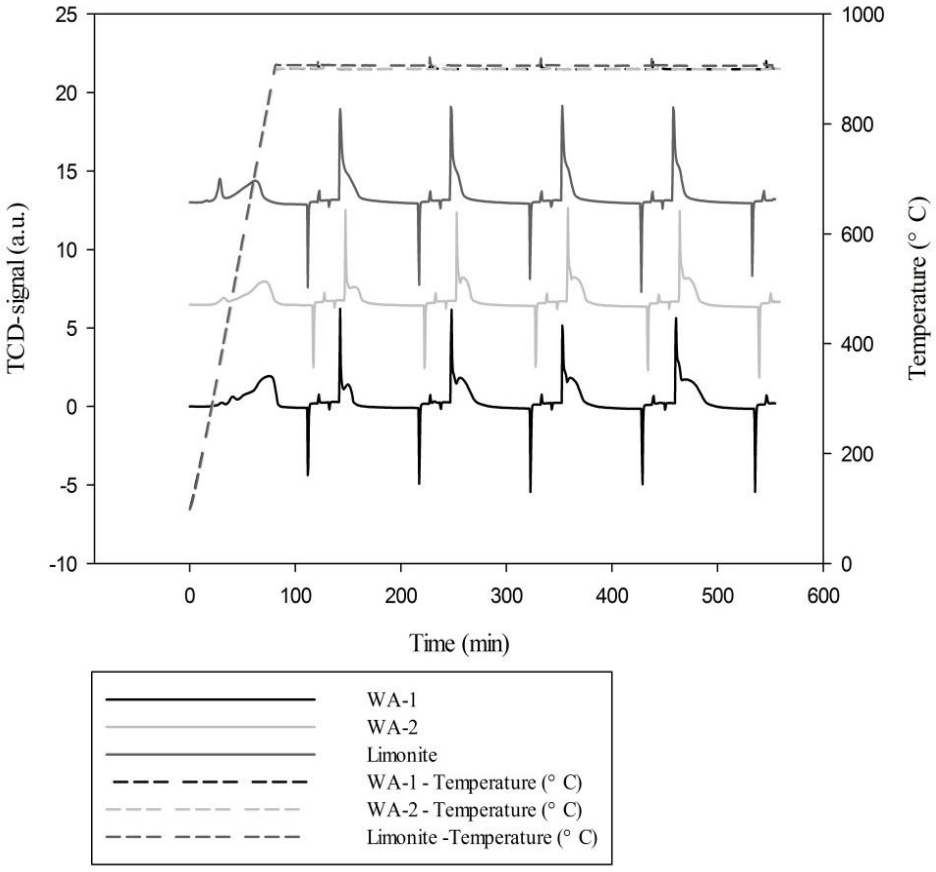


**Figure 5. TPR/TPO measurements of five cycles**

The reduction of the OC occurred progressively as the temperature was increased during the first cycle. In Figure 6, a few peaks can be seen during this first reduction period. It can be seen that the WA-2 sample has two peaks and this corresponds to findings in the literature [36, 37] which state that this is due to the reduction of $Fe_2O_3$ to $Fe_3O_4$ and $Fe_3O_4$ to Fe. Limonite shows three peaks and the first small peak may be due to presence of other oxygen carrier materials. The WA-1 sample displays other unstructured peaks as evidenced in Figure 6 and could be due to other $Fe_2O_3$ reduction paths as discussed in literature [35].

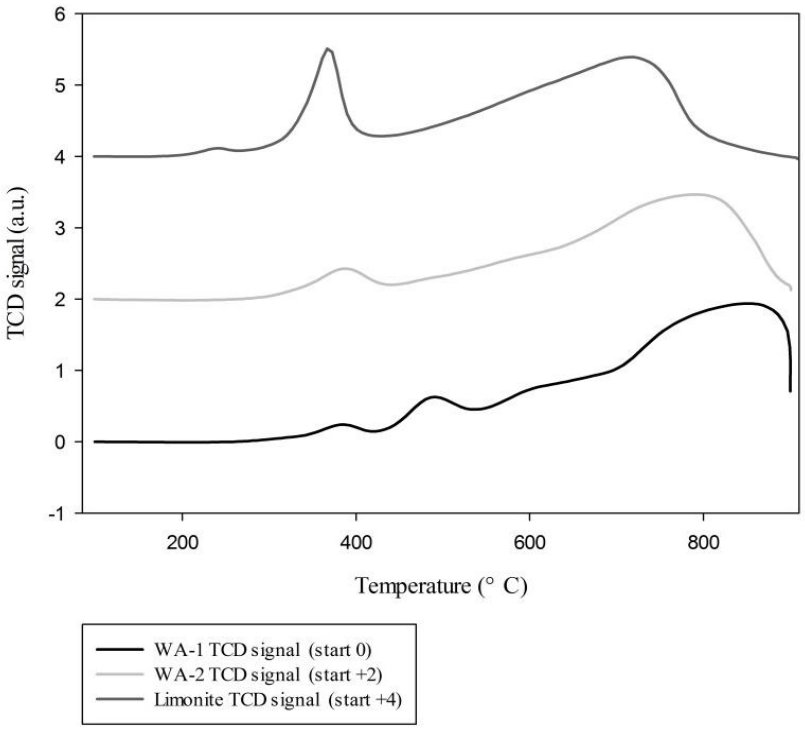


**Figure 6. TPR/TPO measurements, first cycle reduction**

It can be seen that Limonite is reduced at a faster rate and at lower temperature compared to the WA-1 and WA-2 samples. The first peak appears to be around 380°C for both the WA-1 and WA-2 while Limonite's first peak was at 250°C. The large, last peak for Limonite was at 720 °C, while this was at 800 °C for the WA-2 sample and 860 °C for the WA-1 oxygen carrier. Magnacca et al. (2003) showed that the two peaks occur at 376 °C and 627 °C in TPR measurement of α-$Fe_2O_3$ with 5% $H_2$ in Ar at a flow of 40 ml STP [36]. Neither the WA-1 nor WA-2 OCs was completely reduced when the final temperature was reached, whereas Limonite was almost fully reduced when the temperature was 900 °C.

The large peaks found in the 2$^{nd}$ to 5$^{th}$ reduction cycle during the 900 °C isothermal period is due to signals generated from the change in gases and reduction of the OC. It is possible to distinguish the presence of more than one peak in this part. The first part in this peak is due to the change in gas and is replicable for each reduction cycle while the other peaks experience changes in each cycle. Using peak deconvolution to separate the peaks, three peaks during the reduction period are distinguishable, with the first attributed to the change in gas while the other two attributed to the reduction of the oxygen carrier. Figure 7 shows the presence of

three peaks for the 2nd reduction of Limonite, the first being the peak due to the change in gas, which is tall and narrow while the latter two had lower intensities but covered a wider area. This is in agreement with other findings [36, 37].

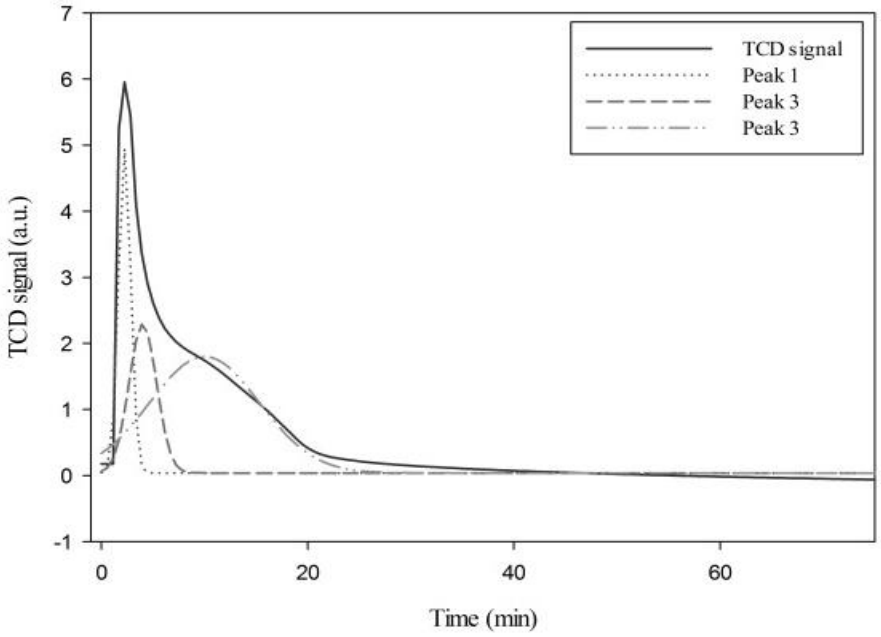


**Figure 7. TPR/TPO measurements 2nd cycle of Limonite, with calculated peaks**

The reduction capacity of the oxygen carriers can be represented by the area below the reduction peaks while reactivity can be inferred from the height in the peaks. The 2nd to the 5th reduction reactions are plotted for the three OCs in Figure 25 to Figure 27 in the Appendix. The reduction capacity increased for WA-1 and WA-2 for each cycle as evidenced by the increasing area below the reduction peaks. The capacity of the WA-1 OC increased after each cycle and this is probably due to structural changes and at the 5th cycle the WA-1 showed the largest capacity of the three studied OCs. Limonite on the other hand showed a larger capacity in the beginning with a subsequent decline in the capacity to a constant value in cycles 3-5. For both the WA-1 and WA-2 samples, the reactivity and capacity was the largest at the 5th cycle. Limonite had the highest peak values while WA-1 had the second highest and WA-2 had the lowest reactivity.

## 4.2 TGA – Redox Reaction with Coal

The measurements performed in the TGA were recorded from 200 °C. The OC samples were fresh samples having different moisture content. In the preheating stage, there was loss of moisture from the fresh OC and coal. The OC would only lose moisture in the first cycle, whereas coal would lose its moisture content in each of the cycles. Therefore, the amount of moisture-free OC in the measurements varied. The measurements performed in the TGA were recorded from 200 °C onwards. The purpose of this experiment was to determine the OC reactivity and stability over multiple redox cycles with coal.

The WA-1 OC showed a quick drop in mass in the initial 10 minutes of the first cycle as can be seen in Figure 8. This loss is due to evaporation of moisture and gasification of coal which proceeded to react with the OC. After the first cycle, the reduction and oxidation patterns were stable and replicable. WA-1 lost 20 mg (4 %) from the initial 500 mg in the first cycle and had a steady mass of 480 mg in the next four cycles. Other studies have also showed that $Fe_2O_3$ did not lose its mass over the multiple redox cycles [50].

The WA-2 OC showed a larger drop in mass in the first cycle, but stabilized to a repeatable pattern for the next four runs, similar to the WA-1 OC. The WA-2 sample lost 40 mg of mass (8 %) after the first cycle, but then showed a steady amount of 460 mg mass for the subsequent cycles. The $Fe_2O_3$ content of the WA-2 sample was 9 % less when compared to the $Fe_2O_3$ content in the WA-1 sample.

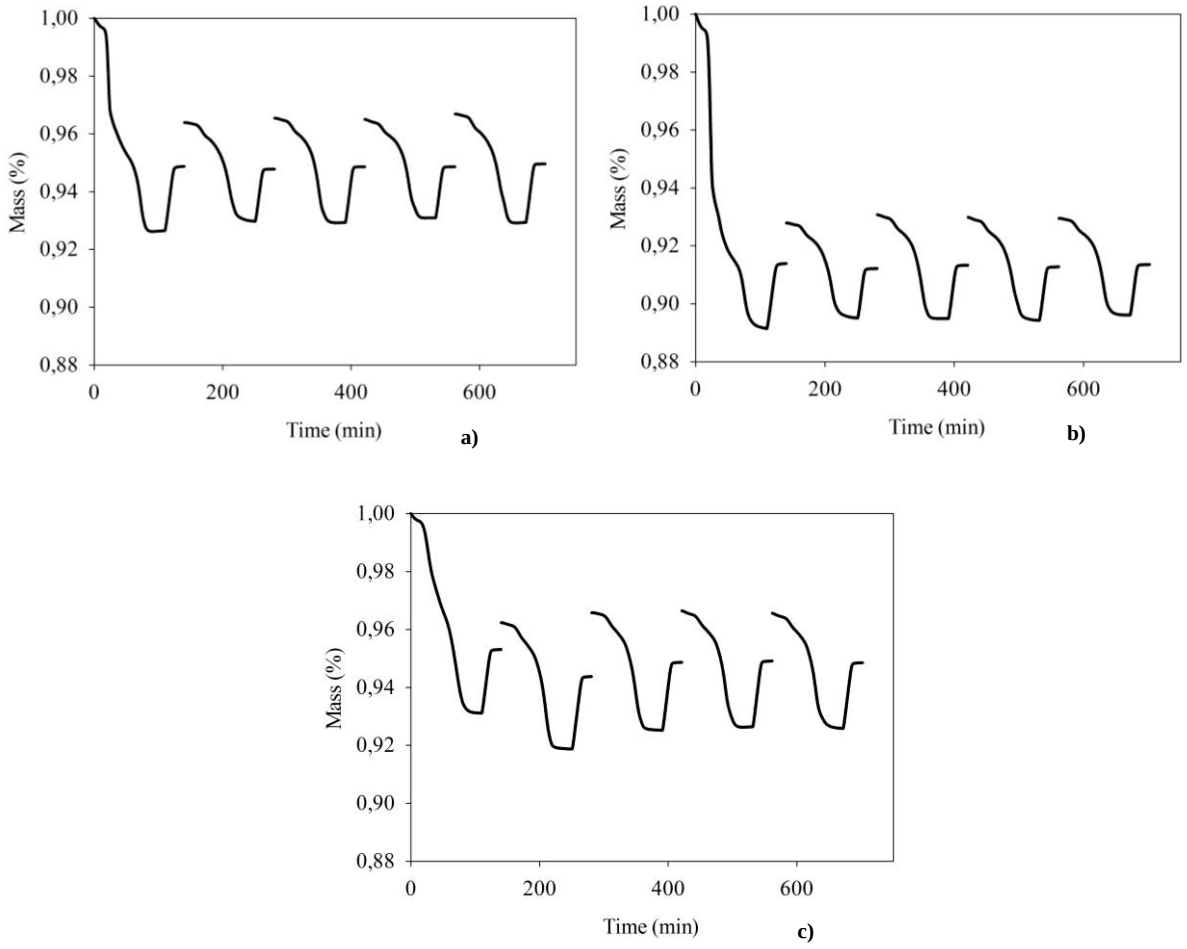


**Figure 8. TGA measurements of a) WA-1, b)WA-2 and c) Limonite for 5 cycles**

Limonite lost moisture in the first cycle, but it also lost a small amount of moisture in the second cycle, creating lower values for the second cycle as can be seen in Figure 8 c). The loss of moisture was not as fast when compared to the other two samples at 200 °C. Limonite lost 34 mg of mass (6.8 %) in the first cycle, but it also lost 1 mg (0.2 %) in the second cycle. The redox pattern was stable beyond the second reaction cycle. Limonite had 20 % less $Fe_2O_3$

compared to the WA-1 sample. The differences in the loss of moisture in each of the OCs could be due to the different ways that water was bonded to the OC.

A comparison among the different OCs was carried out and can be seen in Figure 9. An assumption was made that all the OCs would show a steady pattern from the second cycle. The samples were also compared with a sample of fresh WA-1 which was reacted with coal under steam gasification. The coal was fully converted in all cases and this is supported by the absence of a mass change at the end of the reduction section as shown in Figure 9 b) were the mass change rate is depicted.

The results show that Limonite had the largest loss/gain in mass at the fastest rate among the three tested OCs. The results obtained here is similar to that from the TPR/TPO section whereby Limonite showed the highest reactivity. The WA-1 and WA-2 samples had almost identical weight loss/gain patterns. One run with steam was also evaluated using the WA-1 sample and the pattern was similar, except for the gain in mass during the reduction reaction. Coal was gasified at a faster rate and at an earlier temperature with steam compared to when $CO_2$ was used. This is evident by a higher mass change peak that was shifted to the left in Figure 9 b). and it has been shown in the literature that steam has a positive effect on the gasification of the coal [19].

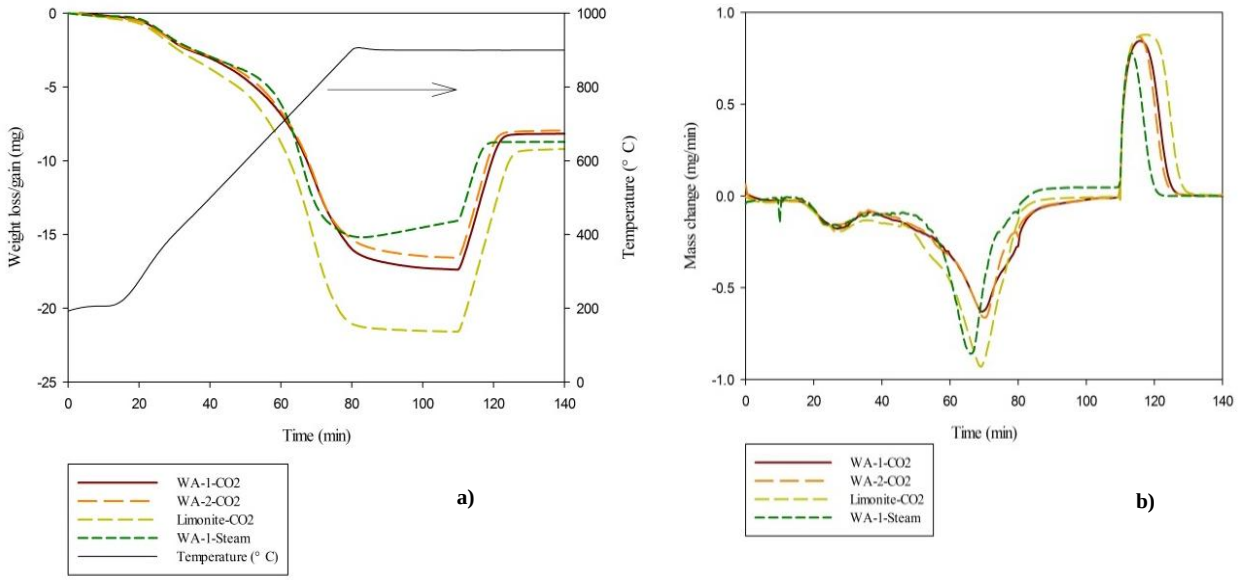


**Figure 9.Comparison of the 2nd cycle of different samples, a) mass change and b) rate of change**

Figure 10 shows another comparison of the second cycle, wherein the WA-1 and calcined WA-1 samples are compared. The comparison showed that there was a difference between the sample used in presence of steam compared to when $CO_2$ was used. The sample in presence of steam had higher reactivity, probably due to faster gasification of the coal. A slight difference could be seen between the calcined and fresh samples. The calcined sampled showed a higher reaction rate compared to the fresh sample both in presence of steam and $CO_2$ with the most evident difference being between the two samples in $CO_2$. Both the oxygen carriers in the steam runs showed an increase in mass at the end of the reduction cycle,

showing an oxidation of the OC. This may be due to oxidation by steam on the surface of the particle, on which a greater extent of reduction would have occurred as it was the closest to the coal and its gasification products.

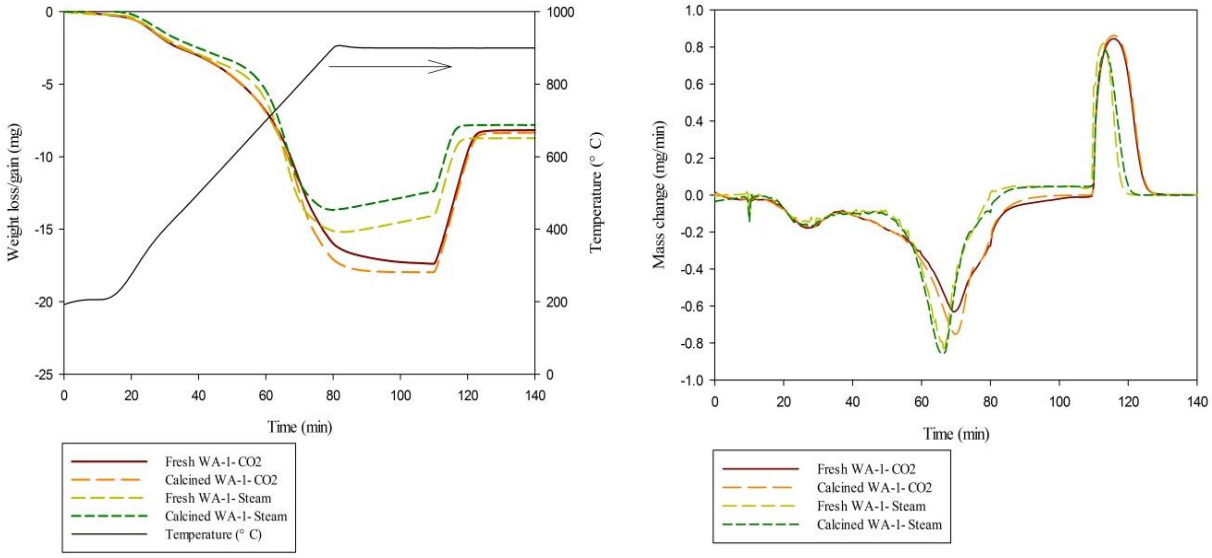


**Figure 10. Comparison of the 2nd cycle of WA-1 samples, both in mass change and the rate of change**

### 4.2.1 SEM Images of the Fresh and Used OC

The fresh samples were first characterized using SEM. The surface of the WA-1 and the WA-2 samples consisted of a thin layer of small particles and this can be seen in Figure 28 a)-b), and Figure 29 a)-b) in the Appendix. Figure 31 in the Appendix shows that the calcined WA-1 sample has a surface covered with small coalesced particles. The fresh Limonite sample showed a much more porous structure with the presence of a lot more fines as depicted in Figure 30a)-b) in the Appendix compared to all the other samples. It appears that the surface area of the WA-1 and WA-2 oxygen carriers is much lower than Limonite, which could explain Limonite's better performance during the TPR/TPO and TGA experiments. The surface area was considerably larger for Limonite OC than for both WA-1 OC and WA-2 OC as will be shown by the ASAP measurements of the fresh samples in Table 6 further down in this report, confirming the reasoning for the enhanced reactivity of Limonite.

The used WA-1 sample also showed grain coalescence as evidenced in Figure 28 c)-d) in the Appendix. The fresh WA-1 sample appears rougher, while the used sample is smoother. The WA-1 particles used in steam for the 2 redox cycles displayed formation of cracks, as shown in Figure 28 c)-d) in the Appendix which would provide larger specific surface area leading to higher reactivity.

The change in the surface of the WA-2 sample is very small. Figure 29 c)-d) in the Appendix shows that the surface is covered in small grains after 5 cycles in the TGA. After the 5 runs in the TGA, Limonite's physical appearance had changed and the surface was covered with more particles as shown in Figure 30 c)-d) in the Appendix.

Very little ash deposition was evident on the particles and this was expected due to the small amount of ash present in the Yallourn coal. Agglomeration of the particles was not evident and this is supported by the fact that $Fe_2O_3$ has a melting point of 1500 °C. Other studies showed that sintering of the grains were not present in experiments using $Fe_2O_3$ with a different Victorian brown coal [50]. The surface of the three OCs in this study had changed due to conditioning and grain coalescence relative to the fresh particle.

The calcined WA-1 sample in Figure 31 in the Appedix showed a very smooth surface with few small particles on it. After the 5 redox cycles, the surface had become less smooth and more particles appeared on the surface which would give rise to a slightly larger surface area and more reactive sites. The calcined WA-1 sample used in 2 redox cycles with steam showed less particles on the surface than the one used in 5 cycles with $CO_2$. The calcined sample, as depicted in Figure 31 a)-b) in the Appedix, shows a smother surface with less sharp edges than for the fresh WA-1 as can be seen in Figure 28 a)-b) in the Appendix. The difference shows that calcination results in a physical change of the oxygen carrier morphology.

### 4.2.2 EDX Analysis of fresh samples and samples in the TGA

It is important to understand the extent of interaction between the ash formed from thermal treatment of coal and the OC in a CLC unit as this can give rise to agglomeration problems, loss of the oxygen carriers' reactivity and bed defluidization in a fluidized bed reactor. Yallourn coal contains very low amounts of ash, and therefore the extent of ash interaction should be very small. It is impossible to compare the surface composition of the same particles before and after the experiment. Since the OCs were natural ores, their composition were highly heterogeneous leading to differences in the composition of each particle. Therefore, multiple samples were analysed and the spectra closes to the average are shown in Figure 11.

It was found that there was very little change in composition between the fresh and used samples, especially for the WA-1 and the WA-2 samples as can be seen in Figure 11. The Limonite OC loses very small amounts of S, and gains very small amounts of Ca as shown in Figure 11, where the small increase of Ca could be due to ash interaction. Limonite sample showed a decrease in oxygen, which could be due to loss of structurally-bound water in the first redox cycle in the TGA.

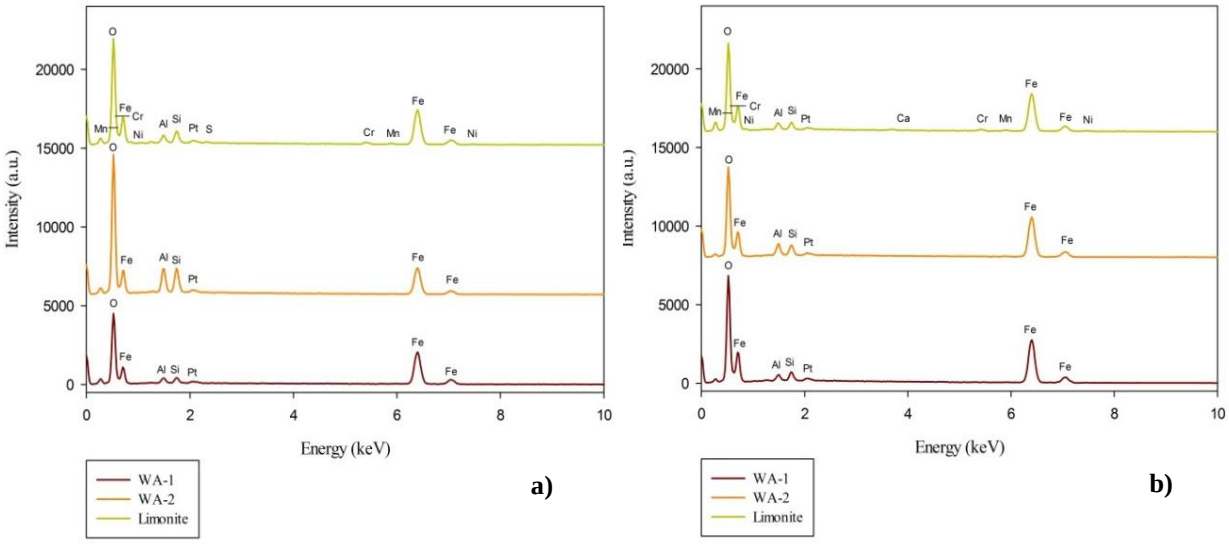


**Figure 11. Electron Dispersive Spectra of a) Fresh samples of OC and b) Used sample after 5 cycles in TGA**

The calcined WA-1 sample showed no change between the used and new sample based on the EDX evaluation as can be seen in Figure 33 in the Appendix. It also showed very small differences between the fresh and calcined sample when comparing Figure 32 and Figure 33 in the Appendix.

For all the OCs, no significant changes could be detected in the EDX which means that ash interaction with the OCs were not significant.

### 4.2.3 XRD Measurements of fresh samples and samples in the TGA

The fresh samples showed low peak intensities, with the WA-1 sample being the one that displayed the highest intensity for a fresh sample and was the most crystalline sample among the other fresh OCs as shown in Figure 12 and Figure 13. The unused calcined WA-1 OC sample showed very high peak intensities in Figure 12 b), indicative of a high degree of crystallinity. The Limonite sample generated the peaks with the highest intensity after the 5 reduction cycles compared to the other two fresh samples. The WA-2 sample did not show any change in composition after 5 cycles except for a change in intensity and that more defined peaks were evident as can be seen in Figure 13 a). The used calcined WA-1 sample did not show any big changes except for a loss in intensity, compared to the unused sample as depicted in Figure 12 b). Used Limonite showed the presence of $SiO_2$ and $Fe_2O_3$ whereas the fresh one only showed $Fe_2O_3$. However, the EDX analysis shows that Limonite has small amounts of Si in the fresh sample as well. As Limonite was the least crystalline sample, peaks for $SiO_2$ may not have been detected in the fresh sample. The fresh WA-1 sample was found to be a mixture of $Fe_2O_3$ and Goethite ($FeHO_2$). After the redox cycles, no $FeHO_2$ could be detected as it was converted to $Fe_2O_3$. The loss of moisture as shown in the TGA supports this observation. It can also be seen that there is significant overlap between the $Fe_2O_3$ and $SiO_2$ peaks for all three OCs. All three samples indicated the presence of Fe, O and Si in the EDX analysis, so an assumption that both $Fe_2O_3$ and $SiO_2$ can be found in the samples are reasonable

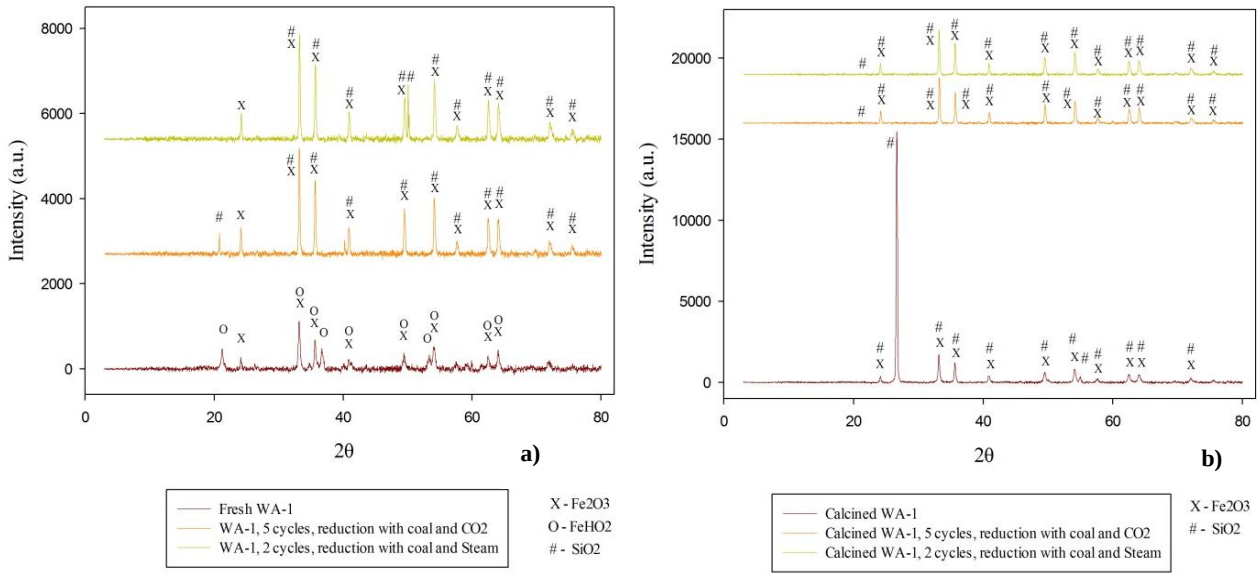


**Figure 12.XRD measurements of a) WA-1 and b) Calcined WA-1**

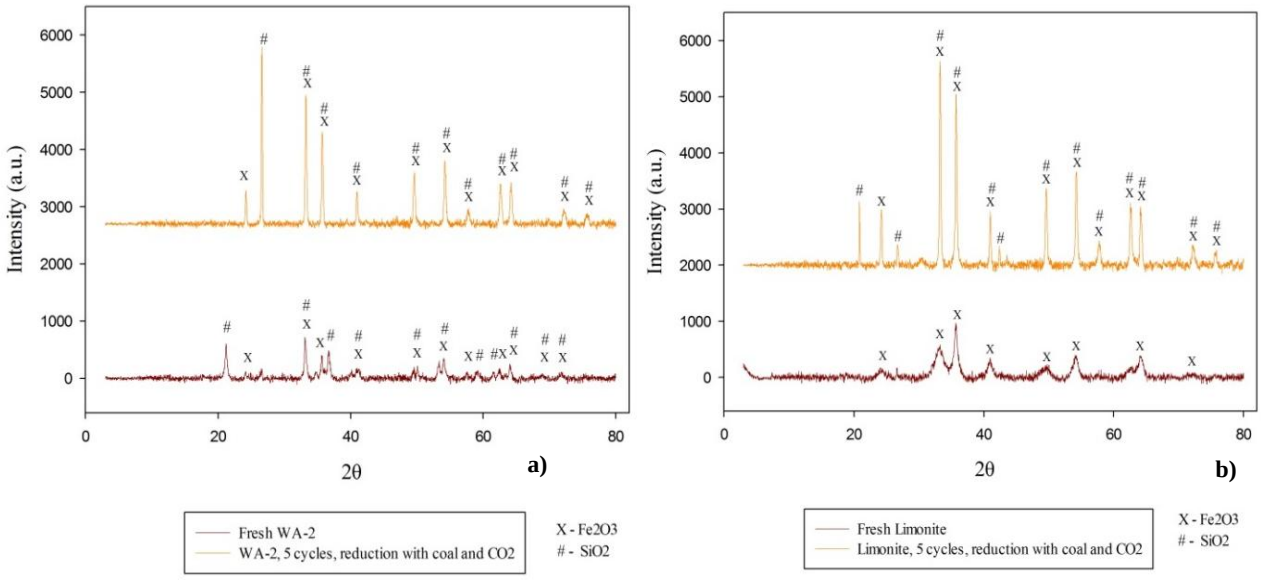


**Figure 13.XRD measurements of a) WA-2 and b) Limonite**

## 4.3 Fluidized bed reactor

The results from the fluidized bed were analyzed based on the composition of the outflow gases. Figure 14 shows the outflow composition of the generated gases, for the three fresh oxygen carriers.

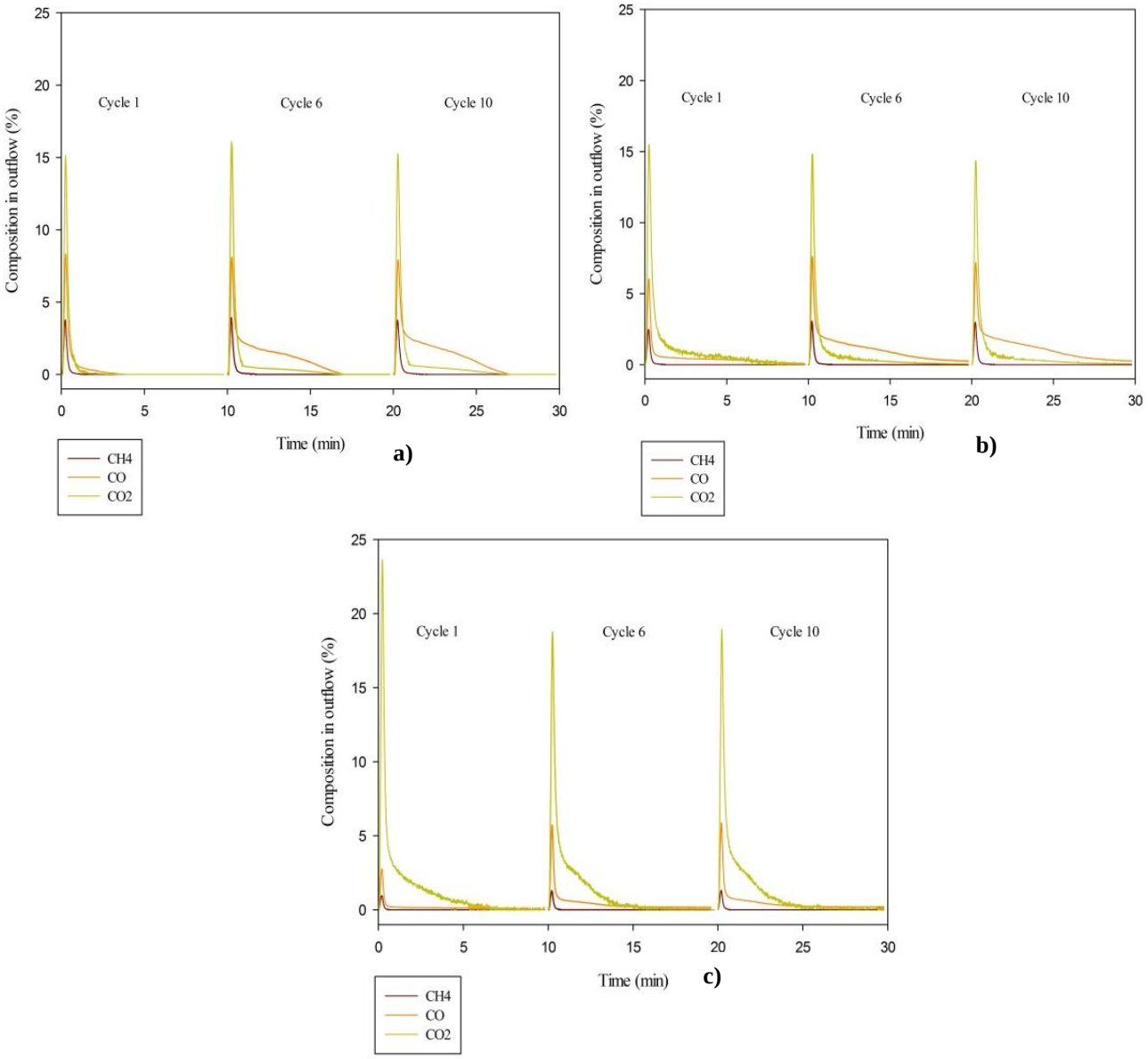


**Figure 14. Produced CO, CO2 and CH4 out from the fluidized bed reactor with a) WA-1, b) WA-2 and c) Limonite**

In the WA-1 and WA-2 experiments, a small decrease in the concentration of $CO_2$ can be seen with an accompanied increase in CO with progressing experiments. Limonite had showed a very high amount of produced $CO_2$ and low amount of CO in the first cycles, but lesser amounts of CO was converted as the cycles continued resulting in a lower $CO_2$ concentration in the outflow, similar to that observed with the WA-1 and WA-2 samples indicating decrease in $CO_2$ conversion. The $CO_2$ conversion was calculated as Equation 11 below shows.

$$CO_2 - Conversion = \frac{F_{outlet} \int_1^n x_{CO_{2-production}}}{F_{outlet} \int_1^n x_{CO_{2-production}} + x_{CO} + x_{CH_4}} \times 100 \qquad (11)$$

Where the $x_{CO_{2-production}}$ was found with Equation 12

$$x_{CO_2-production} = \frac{F_{CO_2-outflow} - F_{CO_2-fluidizing}}{F_{outlet}} \quad (12)$$

Here, $x_{yy}$ denotes the fraction of the gas of interest and the $F_{outlet}$ is the molar outlet flow. The $F_{CO_2-outflow}$ is the molar outflow of $CO_2$ and the $F_{CO_2-fluidizing}$ is the flow of $CO_2$ used for fluidizing the bed. $F_{Carbon\ in\ fuel}$ is the amount of carbon contained in the fuel. The carbon conversion, $X_C$ was evaluated using Equation 13 below which has been used by Zhang et al. (2013)[60]

$$X_C = \frac{F_{outlet} \int_1^n x_{CO_2} + x_{CO} + x_{CH_4}}{n_{Carbon\ in\ fuel}} \quad (13)$$

The carbon conversion shows how much of the carbonaceous matter in the fuel has been converted into gases. With the carbon conversion, the carbon conversion rate, $r_C$, can be found using Equation 14. This show how fast the carbonaceous matter converts to gaseous species.

$$r_C = \frac{1}{W}\frac{dW}{dt} = \frac{1}{1 - X_c}\frac{dX_C}{dt} \quad (14)$$

All the OCs showed a decreasing trend with respect to $CO_2$ conversion as the cycles progressed. This is clearly displayed in Figure 15 showing the amount of produced $CO_2$ compared to the total carbonaceous gases generated from the coal. In this figure it can also be seen that there is a large difference between the $CO_2$ conversions of the three OCs, with Limonite giving the highest concentration of $CO_2$ relative to the carbonaceous gases.

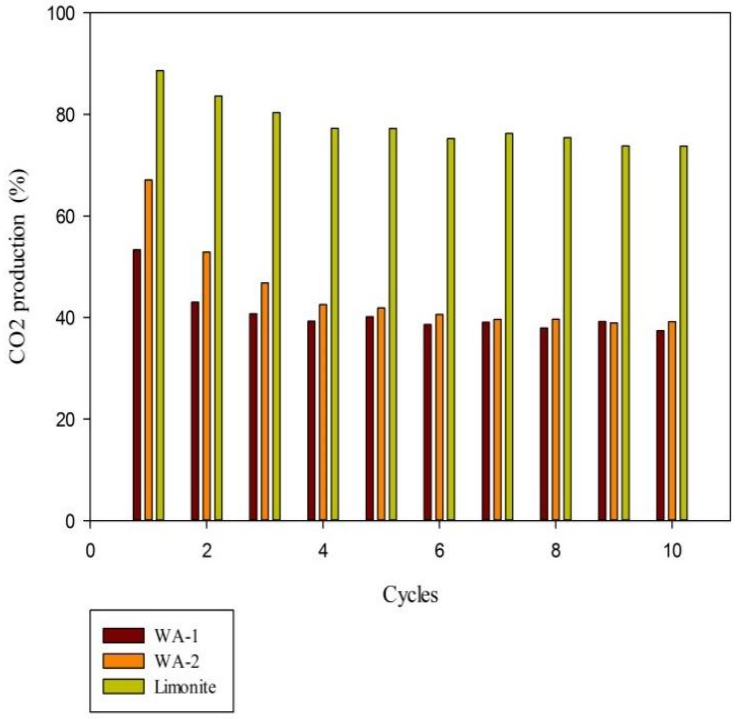


**Figure 15. $CO_2$ conversion compared with produced CO, $CO_2$ and $CH_4$**

The carbon conversion is similar for all the OC but an increase can be seen from the first cycle to the last as depicted in Figure 16 especially for the WA-1 and WA-2 samples. Limonite shows a small increase. Zhang et al. (2013) obtained carbon conversion in the range of 82 % to 95%, with the same experimental setup and coal type [60]. In this study the carbon conversion in presence of the WA-1 sample was only 44 % in the first cycle but around 92 % for the last few cycles except for cycle 8 where it is 99%. This could be due to differences in carbon present in the coal added to the reactor. The reason for this is that coal is highly heterogeneous and its composition varies from particle to particle. The carbon conversion of the WA-2 sample increased from 73 % to 94%. Limonite showed the most stable behaviour with a 75 % carbon conversion in the first cycle and 85 % in the last.

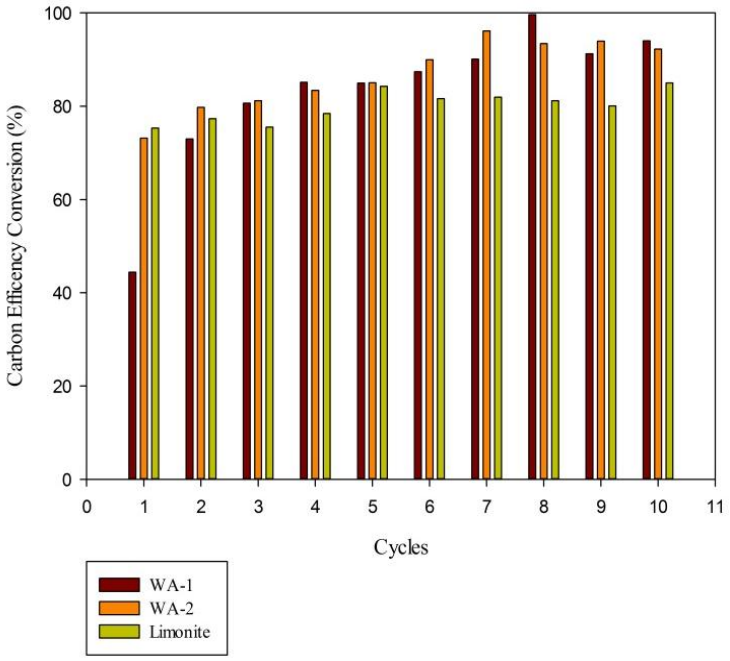


**Figure 16. Carbon conversion of 10 cycles for three oxygen carriers**

The carbon conversion rate in Figure 17 shows that the WA-2 almost always had the lowest values, and the peak value for all the cycles was in the range of 1.64-1.94 $min^{-1}$, where only three cycles are depicted in Figure 17. The WA-1 sample showed the highest values and had a range of values between 1.98-2.37 $min^{-1}$ for all the cycles. Limonite had peak values between 1.79-2.0 $min^{-1}$. Zhang et al. (2013) showed peak values for the carbon conversion rate to be in the range of 1.2-1.5 $min^{-1}$ for three different OCs used in their study [60].

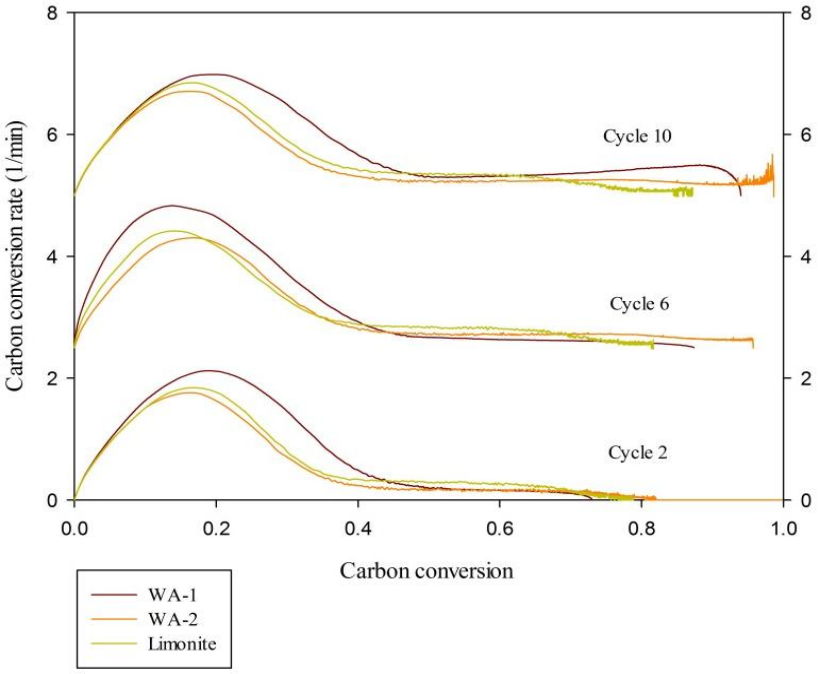


**Figure 17. Carbon conversion rate of the three OC, at 3 different cycles**

### 4.3.1 SEM Images of Fresh and Used Oxygen Carriers

SEM analysis was carried out on the three used OCs which were removed from the fluidized bed after the 10$^{th}$ reduction. The used sample was therefore in its reduced form. None of the OCs showed any signs of agglomeration but some particles showed evidence of crack on their surface. SEM images of the WA-1 sample are depicted in Figure 34 in the Appendix together with pictures of the fresh WA-1 sample which is the same as the one from the TGA experiments.

There were small cracks in the used WA-1 particles and the surfaces are covered in more fines. The used WA-1 sample appears a bit rougher than the fresh WA-1 sample but no significant difference can be seen. There was no noticeable change in the WA-2 sample as shown in the SEM pictures as shown in Figure 35 in the Appendix. The Limonite sample in Figure 36 in the Appendix shows a loss of porosity and some of the fine particles on the surface appear to have coalesced. The reduction in porosity can explain the loss in reactivity which resulted in lower concentrations of $CO_2$ generated as can be seen Figure 15.

### 4.3.2 EDX Analysis of samples used in the Fluidized Bed Reactor

EDX spectra of the samples can be found in Figure 18 from which it was found that there was no significant change in composition of the used OCs compared to the fresh OC. The only change that could be seen was a small gain in Mg for all the samples, possibly from the coal ash. The small amount of Sulphur found in the fresh Limonite sample as seen in Figure 11 a) could not be found in the used one. The amount of Mg and also S are so small that a conclusion that there is significant ash interaction cannot be drawn.

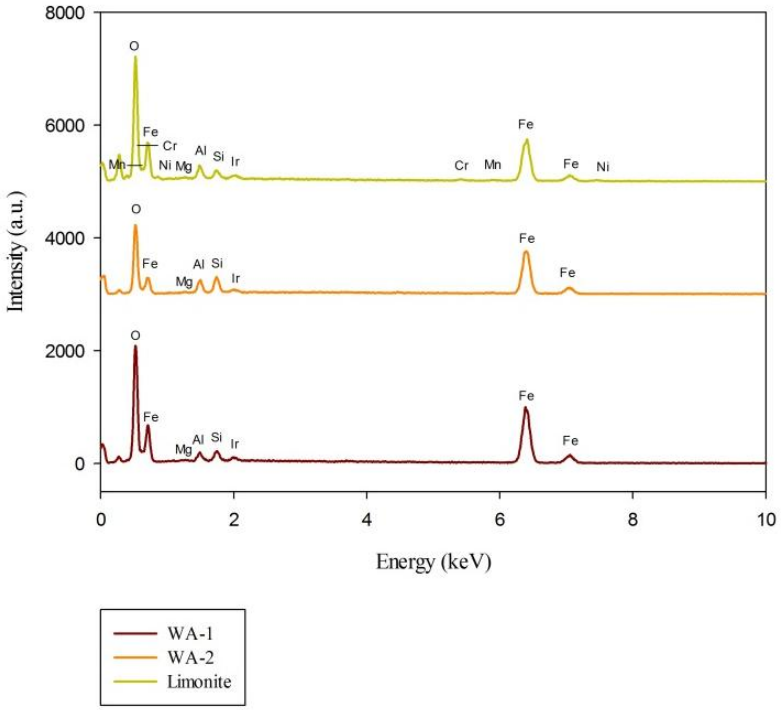


**Figure 18. EDX measurement of the three Oxygen carriers from the fluidized bed reactor**

### 4.3.3 XRD Analysis of samples from the Fluidized Bed Reactor

The XRD analysis of the OC samples after the 10$^{th}$ reduction reaction is depicted in Figure 19 and shows the presence of $Fe_2O_3$, $Fe_3O_4$ and $SiO_2$. These were expected due to the OCs being sampled in its reduced form. The only change relative to the fresh sample was that the WA-1 sample no longer had Geothite ($FeHO_2$) and that $SiO_2$ was found on the Limonite samples. As mention before, the fresh Limonite sample could have contained $SiO_2$ even though it was not found in the XRD analysis of the fresh sample. The presence of $Fe_2O_3$ shows that the sample is not fully reduced, and the sample still has some capacity to be reduced. This is also expected as stoichiometrically the OC was supplied in excess compared to the amount of carbon matter in the fuel and that not all of the fuel had reacted with the OC.

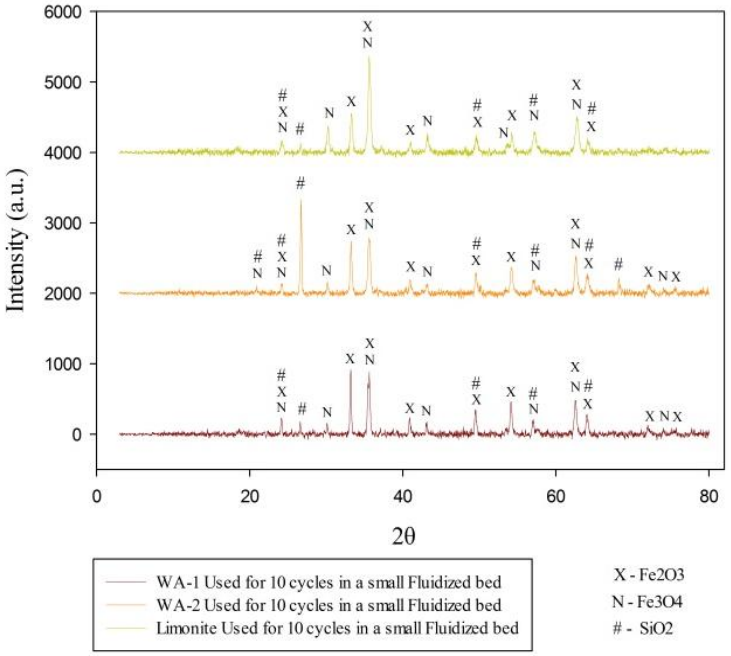


**Figure 19. XRD measurements of the three Oxygen carriers from the fluidized bed reactor**

### 4.3.4 ASAP measurements of the fresh and the used particles

The BET surface area in Table 6 shows that the fresh Limonite particles had a larger surface area than the other two OCs. Also, the used Limonite particles from the FB reactor experiment still had the largest surface area. The surface area of the used samples was significantly reduced compared to the fresh samples as can be seen in Table 6. This could be the reason for the reduced reactivity of all the OCs from the FB experiments, as a reduced surface area would result in a reduction of active sites for reaction with the gas.

The fresh WA-1 and WA-2 samples had a similar order of magnitude for the total pore volume as can be seen in Table 7. The total pore volume at adsorption was measured for pores having an average diameter of 17.0-3000.0 Å. The fresh Limonite sample had a very large pore volume, but this was also reduced after 10 runs in the FB reactor. Also, the WA-1 and WA-2 OCs showed a reduction in pore volume after 10 runs in the FB reactor, which would suggest that the pores of interest in the OC samples had shrunk during reduction and oxidation.

The average pore diameter for the different OCs can be seen in Table 8 below. The fresh samples showed similar patterns in pore diameter as the BET surface area, where the Limonite sample had the largest pore diameter while the WA-1 sample had the smallest average value. After 10 runs in the FB reactor, the WA-2 sample was found to have the largest pore diameter compared to both Limonite and WA-1. All of the three OCs had experienced an increase in their pore diameter after 10 cycles, whereby the WA-2 sample had a doubling in the pore diameter after 10 runs in the FB reactor.

After the 10 redox cycle experiment, all the OCs had a smaller surface area and pore volume but with larger average pore sizes. This is possibly due to coalescence of the grains forming larger grains with bigger pores that would reduce the surface area and pore volume of the OCs. This structural change could be the reason for the lower reactivity of the particles.

**Table 6. Brunauer, Emmett and Teller (BET) surface area of the OC particles**

| *m2/g* | **Fresh OC** | **Used OC in the FB** |
|---|---|---|
| **WA-1** | 43.4282 | 1.9403 |
| **WA-2** | 78.1391 | 5.4033 |
| **Limonite** | 120.821 | 16.3534 |

**Table 7. Pore volume of the OC particles at adsorption**

| *cm3/g* | **Fresh OC** | **Used OC in the FB** |
|---|---|---|
| **WA-1** | 0.020607 | 0.003556 |
| **WA-2** | 0.035349 | 0.014882 |
| **Limonite** | 0.210546 | 0.048984 |

**Table 8. Pore size (4V/A) at adsorption of the OC particles**

| *Å* | **Fresh OC** | **Used OC in the FB** |
|---|---|---|
| **WA-1** | 46.552 | 68.007 |
| **WA-2** | 49.111 | 101.122 |
| **Limonite** | 71.201 | 97.865 |

## 4.4 Process modeling using Aspen Plus

A screen shot of the process models developed are shown in Figure 37 to Figure 40 in the Appendix. The largest species from the reactants CO, $H_2$ and $CH_4$ exiting the gasification reactor was found to be CO. The conversion of CO is therefore used as the key result in this study. The initial settings in the models were 900 °C, 1kg/hr coal, 100kg/hr of $Fe_2O_3$ and a flow of air mixture and Carbon carrier gas (CCG) into the different air reactor and fuel reactor respectively at a rate of 25 L/min.

### 4.4.1 Analysis of the model using only Gibbs reactors

The result of the simulations using Gibbs reactors for the initial settings yielded around 99.9% conversion of CO. The $H_2$ and $CH_4$ had also been totally converted while the $Fe_3O_4$ from the fuel reactor had reoxidized back to its original state of $Fe_2O_3$ after going through the air reactor.

A sensitivity analysis was done whereby different parameters were changed such as

- Temperature: 327-1127 °C (600-1400K) in the fuel reactor and decomposing reactor
- Pressure: 1-15 atm in the fuel reactor and decomposing reactor
- $Fe_2O_3$ feed rate: 50-100 kg/hr into the fuel reactor
- Ratio of $O_2/N_2$ 0.02-10.2 (2-91% $O_2$ in total flow) in CCG into the decomposing reactor
- Ratio of $O_2/N_2$ 0.0002-0.286 (0.02-22.2% $O_2$ in total flow) in the air mixture into air reactor

There is a change in CO conversion with respect to temperature in the Gibbs reactor used for reduction (the fuel reactor). The change in temperature of the fuel reactor, where the reduction of OC occurs, results in an increasing CO concentration at higher temperatures as can be seen in Figure 20. The $H_2$ increases a little with temperature, the $CH_4$ change is so small that it is negligible. The large amount of CO and $H_2$ into the fuel reactor from the decomposition reactor results in an increased amount of CO and $H_2$ in the outflow from the fuel reactor.

When the amount of CO increases at higher temperatures, both into and out from the fuel reactor, the concentration of $CO_2$ decreases as the sum of these concentrations together with $CH_4$ yields a constant value that is related to the carbon content of the coal. The higher the temperature, the higher the amount of CO and $H_2$ produced with fewer amounts of $CH_4$ and $CO_2$ showing temperature dependence.

The conversion of the different gases was very close to 100% for most of the investigated temperatures in the Gibbs reactors, as can be seen in Figure 41 in the Appendix. At very low or high temperatures, the conversion decreases for CO and $H_2$ with the CO conversion being the most sensitive to temperature change as well as having the largest flow. The conversion for CO is around 99.9 % for 350 °C and increases until a temperature of 820 °C after which it decreases for higher temperatures but is still above 99.97 % at 1100 °C.

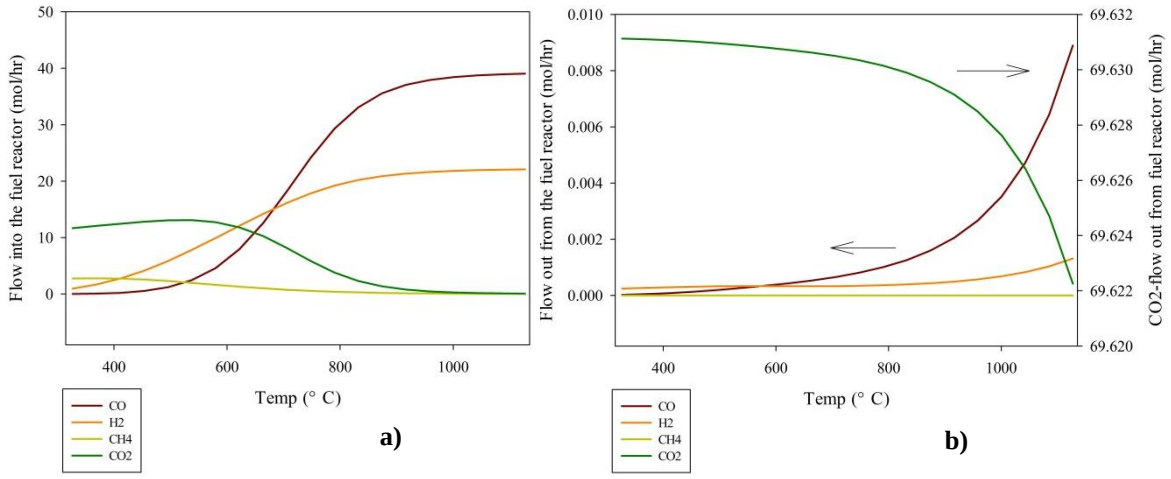


**Figure 20. Change in composition in the a) inflow and b) outflow flow of the fuel reactor, due to temperature change in the fuel reactor and decomposing reactor**

With a change in pressure from 1atm to 15 atm, results were obtained showing that the decomposing reactor was pressure dependent and the fuel reactor was not. A change was detected in the decomposing reactor as can be seen in Figure 21 a) and this presents the outflow from the decomposing reactor which is the inflow to the fuel reactor. Lesser CO and $H_2$ were produced with increasing pressure, but a slight increase in $CH_4$ production could be detected. A change in the pressure did not affect the outflow of CO, $H_2$ or $CH_4$ from the fuel reactor as can be seen in Figure 21 b). This shows that pressure does not affect the reduction stage in the Gibbs reactor even if the inflow to the fuel reactor was changed. The modeling only investigates up to 15 atm in pressure, while this may be higher in a real CLC application.

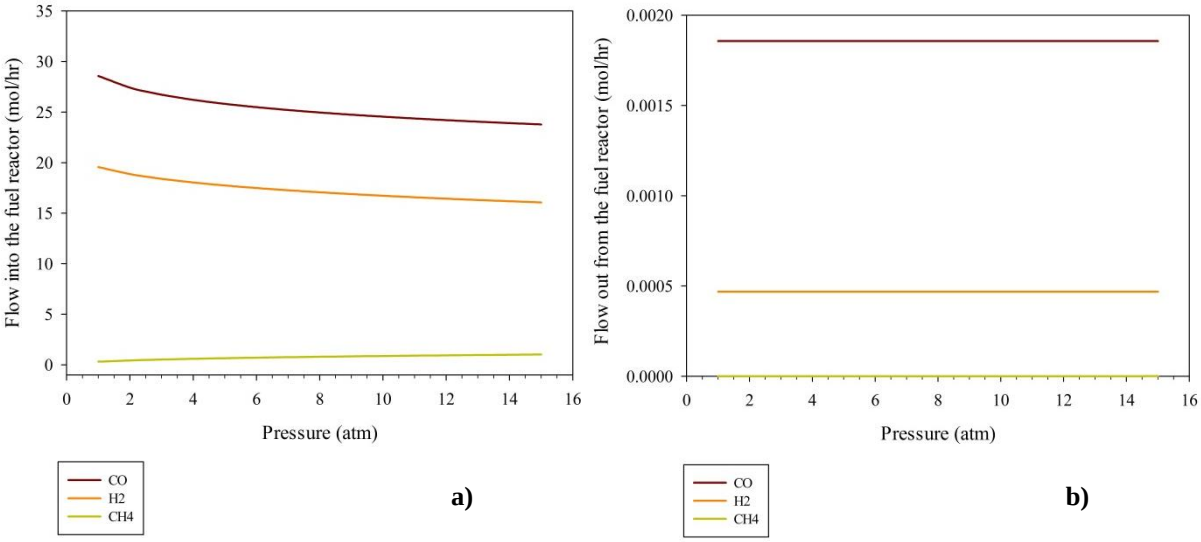


**Figure 21. Change in composition in the a) inflow and b) outflow flow of the fuel reactor, due to pressure change in the fuel reactor and decomposing reactor**

The $CO_2$ composition in the Carbon carrier gas (CCG) flow was varied, by varying the flow rate of $CO_2$, and evaluated as shown in Figure 22. With a high concentration of $CO_2$ in the inflow a higher amount of CO was generated probably due to equilibrium between $CO_2$ and CO. The higher flow of $CO_2$ generates higher flows of CO in the outflow from the fuel reactor as can be seen in Figure 22 b), but $H_2$ and $CH_4$ does not show a significant dependency on the amount of $CO_2$ in the CCG.

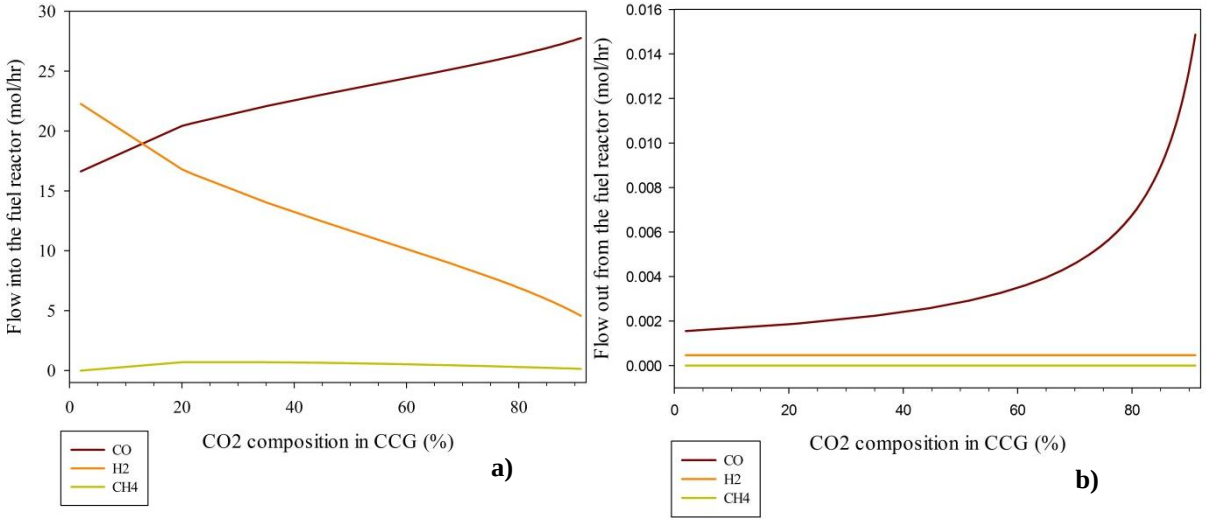


**Figure 22. Change in species of a) inflow and b) outflow of the fuel reactor, when Carbon carrier gas (CCG) composition change**

In the air reactor, the composition of the inflow of air mixture was changed. The flow of $N_2$ is assumed constant, at a rate of 751.62 kg/hr, and inert when changing the flow of $O_2$ and therefore the composition of the flow. A change of $O_2$ concentration in the air flow to the reactor shows that a total conversion of $Fe_3O_4$ can be reached at a concentration of 0.26 % $O_2$

in $N_2$ at the total flow rate of 25L/min, resulting in a flow of 1.96 kg/hr of $O_2$. Compared to the initial condition of 4.2 % $O_2$ resulting a flow rate of 35.64 kg/hr of $O_2$, this is a very low concentration and the initial input had a large excess of $O_2$. The smallest flow of air mixture into the reactor needed for total conversion of $Fe_3O_4$ is 1.301 L/min, consisting of 4.2 % $O_2$ in $N_2$. While this is sufficient from a thermodynamics perspective, it will not be enough in a real application as such a low flow rate would not be able to fluidize the particles.

The feed rate of $Fe_2O_3$ needed to convert most of the coal was 59.2 kg/hr (conversion above 99.99 % of CO). A larger flow of $Fe_2O_3$ did not result in a higher conversion, so the additional 40 kg/hr supplied will theoretically not react in this model.

Both the reduction and the oxidation simulations showed that $Fe_2O_3$ had good thermodynamic reduction and oxidation capacities and that it is a good starting point as an oxygen carrier for a CLC unit. The model shows that the $Fe_2O_3$ could convert almost all of the CO, $H_2$ and $CH_4$ in the fuel reactor while air oxidized the $Fe_3O_4$ to $Fe_2O_3$ in the air reactor.

### 4.4.2 Analysis using different kinetics

The second part of the modelling work with Aspen Plus was done using kinetic parameters from literature. There were a few kinetic parameters for CLC systems in the literature, while some of the evaluated ones are shown in Table 5. Figure 23 shows how the kinetics affects the residence time in the reactor necessary to produce a high conversion of CO.

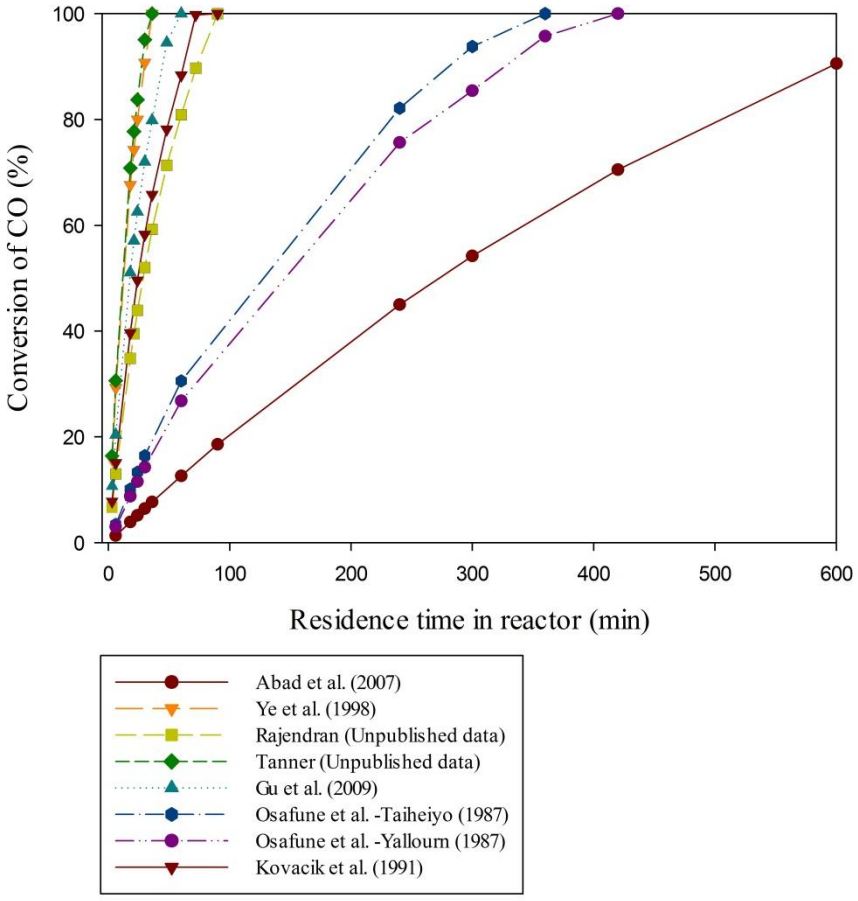


**Figure 23. CO conversion for different kinetic parameters**

Bohnt et al. (2010) had redox kinetics that resulted in a very short residence time and a high conversion compared to all the other kinetics used in this study. It showed that a residence time of 0.00025 seconds was sufficient to reach 100 % conversion. This value was not plotted in Figure 23, but it would have showed a vertical line on the left side of the graph due to large differences with all the other kinetic values used in this study. Kinetic parameters from Abad et al. results in very low conversions even at very long residence times compared to the fastest kinetics by Bohnt et al. (2010) or even gasification kinetics by Ye et al. (1998). The gasification kinetics, except kinetics from Osafune et al, had all reached 100% conversion before 100 minutes, as can be seen in Figure 23. Rajendran's kinetic parameters were obtained from a TGA wherein coal and $Fe_2O_3$ were used. With this kinetics, a conversion of 90 % can be reach at 1.2 hours from the model. Other gasification kinetics gives good conversion at 30 min, for example the gasification kinetics of Yallourn by Tanner. An older study using Yallourn, by Osafune et al. (1988), showed that a residence time of 5.5 hours was required for a 90 % conversion.

A temperature sensitivity analysis for three of the 8 kinetic parameters was done using data from Abad, Rajendran and Osafune which can be seen in Figure 42 to Figure 44 in the Appendix. Higher temperatures resulted in higher conversion, as is expected due the dependence of temperature in the Arrhenius equation. The longer the residence time the higher the conversion. Abad's kinetic parameters were found to be the slowest one with the lowest conversion whiles the values by Rajendran being the fastest one of the three.

Two oxidation kinetic parameters were also evaluated as can be seen in Figure 24. The fuel reactor was a Gibbs reactor resulting in the formation of $Fe_3O_4$ which was sent to the air reactor, the batch reactor with kinetics. There was no difference between the $Fe_3O_4$ conversions with the two different kinetic parameters, indicating that the kinetic is not the rate determining step. If the flow consisted of 21% $O_2$ in $N_2$, a flow of pure air instead of the mixture of air in $N_2$, the different kinetics resulted in a different conversion of $Fe_3O_4$ as can be seen in Figure 44 in the Appendix. Herein, Abad et al. (2007) showed 70% conversion of $Fe_3O_4$ after 420 min of residence time at 900 °C, while the oxidation kinetics from Son et al. (2006) gave a conversion of 80% at 15 min. This indicates that the rate governing stage in the air reactor is the inflow of $O_2$ into the reactor.

The kinetics used in this study are varied, some were based on gasification kinetics while others were developed by researchers at the Department of Chemical Engineering at Monash University. There is a very small amount of kinetic data in the literature on the oxidation and reduction of $Fe_2O_3$ in a CLC setup.

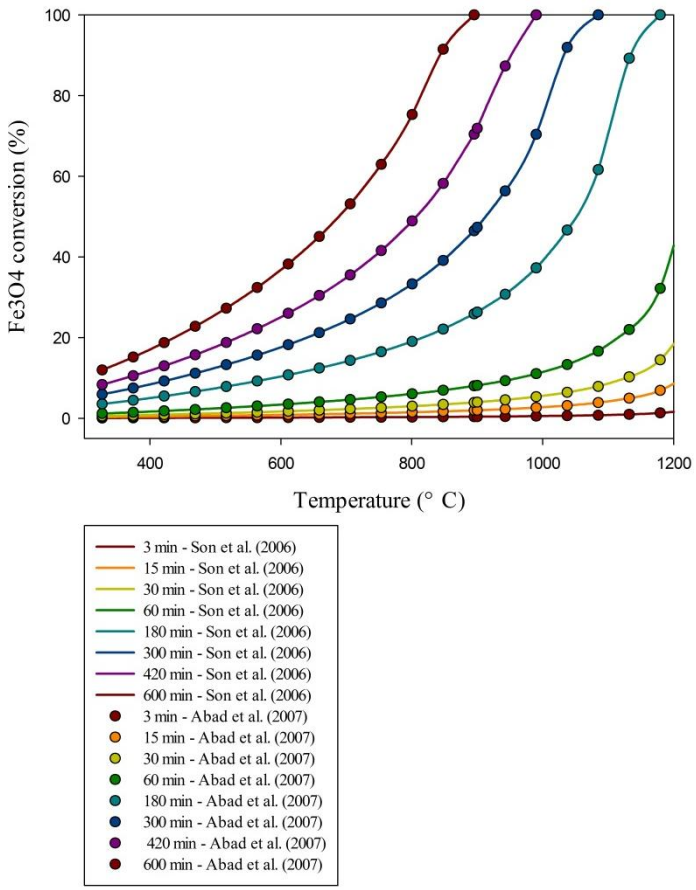


**Figure 24. $Fe_3O_4$ conversion with two different oxidation kinetics in the air reactor**

### *4.4.2.1 Reaction between oxygen carrier and other species*

The fuel stream into the fuel reactor, after the decomposing reactor was divided into two streams. This to evaluate if it was possible to assume that most of the species formed in the gasification stage, except for $CH_4$, CO, $CO_2$, $H_2$ and $H_2O$ used in the reaction, were inert. They did not appear in the reactions mentioned in the Methodology section (A1-A3). The result shows that the species that do not appear in the reduction reactions change only in the range of $10^{-8}$ kg/hr ($10^{-6}$ mol/hr) with a total inlet flow of 22.4 mol/hr. The largest flow in this is $N_2$ from the Carbon carrier gas. All the other species had small flow rates relative to that of $N_2$.

# 5. DISCUSSION

## 5.1 TPR/TPO

An increase in capacity of the three oxygen carriers was progressively seen in the TPR/TPO. This may be due to structural changes during the reduction and oxidation of the oxygen carrier resulting in conditioning of the particle.

Theoretically, since the WA-1 OC contained more $Fe_2O_3$ than the other two, it should have higher capacity. The capacity was also the largest for WA-1 in the $5^{th}$ cycle compared to the other OCs. The reactivity of the three OCs were different, Limonite had the highest peak value after deconvolution and therefore should have the highest reactivity, while the WA-1 showed slightly higher values than WA-2. Limonite contained other species which could act as OCs . Studies have shown that bimetallic OCs display better results than regular $Fe_2O_3$ [32]. With this in mind and that Limonite is also a more porous material than the other OCs used in this study, these would explain the high reactivity of Limonite in comparison to the other OCs.

## 5.2 TGA

Based on the TPR/TPO results, the TGA tests were aimed at establishing that Limonite was the one with the best reactivity. Capacity is not measured in the TGA as the amount of coal added was not sufficient to reduce the OC beyond $Fe_3O_4$. The result was similar, in that the Limonite OC displayed high reduction and oxidation reactivity which could be attributed to the other metal oxides found in the ore and its porous form as already mentioned.

The amount of coal used in each cycle was 10 mg and the ash content of the coal was around 2 % having up to 40 % $Fe_2O_3$ which could act as an oxygen carrier. This would lead to the amount of ash in the sample being 0.2 mg in each cycle, resulting in an increase of 1 mg for a total of 5 cycles. The ash in the sample that does not act as an oxygen carrier is less than 0.6 mg, which is negligible compared to the 500 mg of OC which was added in the beginning.

The mass loss in the beginning of every cycle is due to moisture as the different OC contained different amount of moisture. Since the sample used in the TGA was the fresh OC, the amount of mass used for each sample varied slightly. The shape of the mass loss curve of moisture in the first cycle for WA-1 is similar to the WA-2 samples wherein the loss is quick and at a lower temperature. Limonite shows a weight loss that is not as fast, which can be due to the way the moisture is bound in the particle.

The oxygen carrier particles evaluated with SEM showed that the WA-1 and the WA-2 samples have lower surface areas. The fresh Limonite sample showed a large surface area in the ASAP evaluation compared to the other two fresh OC sample as can be seen in Table 6. The larger surface area of Limonite could explain the better results which were obtained. This is because the larger surface area gives rise to more active sites for reaction with the reducing gases leading to a higher reactivity. Tian et al. (2013) showed that Limonite demonstrated a better reduction performance than most of the other iron ores evaluated in that study [40].

The run using steam for the fresh WA-1and calcined WA-1 samples showed a gain in weight during the end of the reduction cycle. This may be due to oxidation by steam on the surface of

the particle, on which a greater extent of reduction would have occurred as it was the closest to the coal and its gasification products. Steam had a positive effect on the gasification of coal as seen with the few samples which were tested in the TGA. Similar findings to this have been reported in literature [19].

The fresh WA-1 particles showed the formation of cracks after 2 runs in steam. The surface is more uneven after it was used, with the presence of smaller particles in different sizes. This would indicate a higher reactivity from a surface area view point after a couple of cycles. The cracks could be due to the reduction of the fresh particles. No cracks could be seen in the calcined samples as the calcination process increases the thermal and mechanical stability of the oxygen carrier and can be the explanation as to why no cracks could be detected. The samples experimented in the TGA experiences little attrition or mechanical stress and therefore the formation of cracks by these two mechanisms are highly unlikely.

There was very little ash deposition and no agglomeration of the particles in the samples from the TGA. This was expected due to the small amount of ash in the coal. No agglomeration of particles was supported by the fact that $Fe_2O_3$ has a melting point of 1500 °C. Saha et al. (2012). showed that sintering of the grains were not present in their experiment using $Fe_2O_3$ and they did not find any ash interaction with their coal which is another type of Victorian brown coal [50]

The SEM images showed that the small particles on the surface had coalesced. In all the three used OC samples, the appearance of the surface had changed. The sample which underwent the most obvious change was Limonite as shown in Figure 30 in the Appendix. Oxidation is an exothermic process and it is possible that some of the other oxygen carrier components may have melted resulting in it changing its shape.

Both the EDX evaluation and the XRD analysis from the three TGA experiments showed that the fresh and used samples contained the same species, $Fe_2O_3$ and $SiO_2$. The fresh WA-1 sample shows goethite to be present initially in the XRD analysis but this was lost after it was subjected to thermal treatment in the reactor. The loss of moisture in the fresh WA-1 sample causes goethite ($FeHO_2$) to form $Fe_2O_3$ when oxidized. Fresh Limonite showed only $Fe_2O_3$ in the XRD analysis but it is assumed to also contain $SiO_2$ due to Si was found in the EDX analysis, this was not detected because the XRD signal was not clear. A small ash interaction could be seen in the EDX sample for Limonite, where Limonite lost S due to thermal treatment but gained small amounts of Ca, this was not detected in the XRD analysis and is assumed to be a negligible effect. It is also worth indicating that XRD detects only crystalline compounds, and not amorphous compounds.

### 5.3 Fluidized bed reactor

The results from the small fluidized bed reactor show that Limonite is the best of the three OCs in terms of $CO_2$ conversion of the produced gases. This was also found with the TPR/TPO and TGA experiments confirming that Limonite had the best reactivity. Instead of an increase in reactivity over the reaction cycles as the TPR/TPO showed, the result from the FB showed a decreasing reactivity for the first cycles, but then gave a stable value. This is probably due to structural changes where all the OCs showed a lower surface area after 10

runs in the FB reactor. A 100% conversion of CO and $CH_4$ to $CO_2$ and $H_2O$ is not reasonable as the coal was added from the top of the reactor. The coal would devolatilize and gasify as soon as it enters the fluidization chamber and some of these gases would most likely exit the reactor into the gas analyzer without reacting with the OC.

The WA-1 and WA-2 samples show an amount of 40% $CO_2$ in the outflow of produced gases. Even when taking into account the previously mentioned statement, this conversion cannot be concluded as a good result. The conversion values are stable but very low. The Limonite sample had a conversion of 90% of $CO_2$ which is good in the first cycle, but after subsequent cycles the conversion was below 80%.

The concentration of $Fe_2O_3$ in the oxygen carriers does not seem to be a crucial factor in this study, but the porosity is a more important factor, as Limonite shows better results compare to WA-1 which has a higher amount of $Fe_2O_3$ in the sample. Limonite also contained other minerals that could potentially have a positive effect on its reactivity.

The carbon conversion rate was only marginally higher for this study compared to that of Zhang et al (2013) study [60]. The heterogeneity of the coal sample could be the reason to the differences together with the other oxygen carrier used in that study. The carbon conversion rate shows the gasification rate, the reduction of the oxygen carriers should increase that rate. This is due to the reaction between the OC and the gasified products is removing the hindering products of the gasification. The OC with highest reaction rate should therefore show the highest carbon conversion as it removes the gasification products fastest. The Limonite sample showed the most stable carbon conversion and rate over the 10 cycles in the FB and had highest reaction rate in the TGA and TPR/TPO, but still the WA-1 had the highest values. The Limonite sample which had the best reactivity did not show a better carbon conversion rate compared to WA-1, and this needs to be further investigated.

### 5.4 Aspen plus modeling

The Aspen models were developed for a fluidizing bed reactor configuration intended for simulation of a CLC process using $Fe_2O_3$ and Victorian brown coal. The Gibbs model shows the equilibrium outcome while a real reactor will probably have dependence on kinetics, the residence time of particles as well as temperature and pressure. The amount of $Fe_2O_3$ would make a difference in the conversion of the coal in a real case, as more material will have more surface area for the reducing gas to react with. But this did not have a considerable effect in this analysis based on the Gibbs reactors. Changes in conversion over the fuel reactor could be detected due to temperature changes but not due to pressure. The conversion changes for temperature was very small and a conclusion that temperature and pressure will significantly affect the conversion could not be found, due to reaction is based on equilibrium and assumed to go to steady state.

Due to changes in temperature a higher amount of CO could be detected in the inflow to the fuel reactor. A favorable reactor temperature, when evaluating the conversion over the fuel reactor shows that a temperature range between 600-950 °C would give the highest conversions, but outside these ranges the conversion is still high for the Gibbs reactor.

The Chatelier's principle says that the equilibrium concentrations does not depend on pressure, only when the volume changes the effect of pressure is present. This is not the case in our process where one mole CO reacts and form one mole $CO_2$. Hence there should not be a change due to pressure change for the fuel reactor. The pressure change did only give a small change in the decomposing reactor that represented the gasification stage in the reactor. The decomposition reactor shows how solid coal is gasified, giving a volume change. If the Chatelier's principle is used in this part there would be an affect due to the pressure in the decomposition reactor. Roberts et al. (2000) showed little pressure dependency on char gasification, compared to temperature dependency [61]. In this model only a small change could be detected and it is possible that no or larger effect on the gasification will be evident in an experiment. The pressure dependency in a CLC reactor has been shown by Garcia et al. (2005). They showed that the reactivity for the oxygen carriers did decrease when the total pressure increased [62].

The gasification kinetics used in this model is not totally representative for modelling a CLC unit with iron ore containing $Fe_2O_3$ together with a fuel like Yallourn coal. There is very little information on reaction kinetics of the oxygen carrier with solid fuels in literature. Therefore the gasification kinetics of coal was used due to it being the rate governing step in the CLC unit. Some of the gasification kinetics was for Yallourn coal, but others were for other coal or char. The kinetics were also obtained using different methods with a variance in the type of reactor such as a single particle reactor, a TGA or a fluidized bed reactor, which will all have an effect on the kinetics. Literature proposes a number of different ways to reduce the $Fe_2O_3$ with many intermediate steps, which could also give different kinetic parameters for each step.

The kinetic parameters generated by Abad et al. (2007) resulted in a very low conversion rate. The gasification stage have been concluded the rate governing stage [19, 22] and reduction kinetics should give a faster reactions than gasification kinetics. But when comparing residence time using the reduction kinetic parameters of Abad et al. (2007) with any gasification kinetics, the residence time is shorter for all of the gasification kinetics. This indicates that a further evaluations with the kinetics from Abad et al. (2007) needs to be done.

The kinetic parameters were primarily from TGA or similar scale equipment, where the particles are in a fixed bed. While CLC typically utilizes a fluidized bed and that the presence of mixing would give an even faster reaction rate. Gasification in presence of oxygen carriers should be faster due to the fact that the reduction of the oxygen carriers consumes the products of the gasification reaction, which are known gasification inhibitors. Due to the presence of oxygen carriers and a fluidized bed reactor, experimental values should be faster than the one found in this model.

Bohn et al. (2013) have kinetics for the reduction of $Fe_2O_3$ in a fluidized bed reactor, but using those values, the residence time in the batch reactor was found to be 0.00025 seconds to reach equilibrium. Comparing these values with Rajendran who has reduced $Fe_2O_3$ with Yallourn coal, that shows a good conversion after 1.2 hours, represents how the kinetic parameters can significantly affect the CO conversion in the model.

The two kinetics evaluated for the air reactor shows identical result with initial composition settings. When the composition of the air inflow increased from 4.2% to 21% of $O_2$, it resulted in a difference between the two kinetics used. This shows that the inflow of $O_2$ of the initial settings will be the rate governing factor. The oxidation is and exothermic reaction and therefore will the reaction be needed to be controlled to not cause large temperature rise, that will affect the particles negative, such as sintering and agglomeration.

When investigating the effect of the inert particles and the oxygen carriers, the result showed that the need for dividing the fuel reactor into a batch reactor and a Gibbs-reactor is unnecessary. The inert species were found to not react with the oxygen carriers in a wider range of conditions. If an evaluation of these reactions is needed, the kinetic parameters and reactions can be added to the model. The Victorian coal in this model has a low amount of ash, nitrogen, and very little amount of sulfur. It is therefore reasonable to assume these as inert components, as the evaluation shows. The ash was assumed from the start to go straight through the reaction as an inert, in a real process parts of the ash will probably affect the CLC process. This could for example react with the oxygen carriers or it can cause the particles to agglomerate and cannot be assumed to be inert in a real case. In this study, the ash content is very low, but if the model is to be used for other coals with higher ash content, then there is a need for including the reaction kinetics of the ash.

# 6. CONCLUSIONS

This study consisted of two parts involving both experimental and modelling aspects. The experimental work is to evaluate the use of three different iron ores as oxygen carriers together with a Victorian brown coal in a CLC process.The modelling part in this study is a preliminary model aimed at simulating the operation of a $10kW_{th}$ fluidized bed reactor system.

The three iron ores showed a stable cyclic behaviour when evaluated using both the TPR/TPO and TGA for five cycles totalling 9.7 hours and 11.7 hours respectively. While the surface morphology of the three OCs in this study changed due to conditioning and coalescence of the grains, these show promising features in terms of reactivity and minimum interaction with the ash from Yallourn coal based on the TGA experiments. Among the three tested minerals, the Limonite sample showed the best redox reactivity compared to the WA-1 and the WA-2 samples. This is due to its highly porous nature and also to a lesser extent due to the content of other minerals in the ore which could act as oxygen carriers. The WA-1 sample showed the largest capacity based on the TPR/TPO experiment and this is due to it having the highest amount of $Fe_2O_3$.

The fluidized bed results showed 80 % $CO_2$ conversion with the Limonite sample, but for both the WA-1 and WA-2 samples the $CO_2$ conversion was 40 % after 10 cycles of operation. The oxygen carriers showed a decreasing $CO_2$ conversion over 10 cycles. The OCs also showed a decreasing surface area after 10 cycles in the fluidized bed which could explain the decreasing reactivity in the fluidized bed reactor. The OC was removed while it was in a reduced state

from the last reduction cycle and showed the presence of both $Fe_2O_3$ and $Fe_3O_4$ in the XRD analysis. This indicates that the OC was not fully reduced as expected because the OC was in excess. The samples did not show any agglomeration but the surface morphology of the oxygen carriers had changed in the form of cracks which could be due to attrition in the fluidized bed. The coal used in this study shows promising results for a future CLC process due to its low ash content, and that no significant interaction could be concluded in this study.

The process model developed using Aspen Plus showed that $Fe_2O_3$ is a good starting point for a CLC unit as an oxygen carrier for use with the Victorian brown coal. An almost complete conversion of CO, $H_2$ and $CH_4$ in the fuel reactor and total conversion of the $Fe_3O_4$ to $Fe_2O_3$ in the air reactor was obtained for the models based on the Gibbs reactors. A number of kinetic parameters were studied in the model with batch reactors, showing 100 % conversion of CO after 0.00025 seconds to 90 % conversion after 5.5 hours depending on the kinetic used. The two different kinetics used in the air reactor did not show any difference for a low flow of $O_2$. With a higher flow of $O_2$ the different kinetics showed a difference in $Fe_3O_4$ conversion showing that the low flow of $O_2$ is rate determining. Further development of kinetics and also comparison between experimental and model predictions needs to be done.

The reduction kinetics used was based on $CO_2$ gasification or reduction of $Fe_2O_3$, but in a future CLC process model both $CO_2$ and Steam gasification and reduction needs to be used to give a proper model for a real CLC plant.

# 7. RECOMMENDATIONS FOR FUTURE WORK

This study involved one experimental part and the other part was process modeling. One of the OCs in the experimental evaluation, WA-1, should be evaluated in further experiments, and in a larger alternating fluidized bed reactor. The experimental part could be extended with:

- The fresh WA-1 showed poor results and a future work using this would be to evaluate the effect of calcination. A smaller particle size is also a possibility as it would give a higher surface area.
- The carbon conversion rate for the different oxygen carriers needs to be further evaluated

Suggestion for further work in process modeling include:

- Change the batch reactor to a fluidized bed reactor and utilizing appropriate kinetic parameters developed for this coal in $CO_2$ and steam and in presence of $Fe_2O_3$.
- Evaluate the effects of process parameters, as pressure, over a wider range.
- Compare the model predictions with experimental data

# 9. REFERENCES


1. Marrero, G.A., *Greenhouse gases emissions, growth and the energy mix in Europe.* Energy Economics, 2010. **32**(6): p. 1356-1363.
2. Mandil, C., *Reducing Greeenhouse Gas Emissions - The potential of Coal*. 2005, International Energy Agency: 9 rue de la Fédération, 75739 Paris.
3. Constantin, F.A. and I. Loredana, *International Multidisciplinary Scientific GeoConference : SGEM : Surveying Geology & mining Ecology Management.* Surveying Geology & mining Ecology Management (SGEM), 2009. **1**: p. 8.
4. Hossain, M.M. and H.I. de Lasa, *Chemical-looping combustion (CLC) for inherent CO2 separations—a review*. Chemical Engineering Science, 2008. **63**(18): p. 4433-4451.
5. Statoil. *Sleipner West*. 2013 17 December [cited 2014 11 May]; Available from: http://www.statoil.com/en/TechnologyInnovation/NewEnergy/Co2CaptureStorage/Pages/SleipnerVest.aspx.
6. Carbon-Capture-Sequestration-Technologies. *Sleipner Fact Sheet: Carbon Dioxide Capture and Storage Project* 2014 21 January [cited 2014 11 May]; Available from: https://sequestration.mit.edu/tools/projects/sleipner.html.
7. Herzog, H. and D. Golomb, *Carbon capture and storage from fossil fuel use.* Encyclopedia of energy, 2004. **1**: p. 1-11.
8. Hoteit, A., A. Forret, W. Pelletant, J. Roesler, and T. Gauthier, *Chemical looping combustion with different types of liquid fuels.* Oil & Gas Science and Technology–Revue d'IFP Energies nouvelles, 2011. **66**(2): p. 193-199.
9. Lyngfelt, A., *Oxygen carriers for chemical looping combustion-4 000 h of operational experience.* Oil & Gas Science and Technology–Revue d'IFP Energies nouvelles, 2011. **66**(2): p. 161-172.
10. Leion, H., T. Mattisson, and A. Lyngfelt, *Use of ores and industrial products as oxygen carriers in chemical-looping combustion.* Energy & Fuels, 2009. **23**(4): p. 2307-2315.
11. Abad, A., J. Adánez, F. García-Labiano, L.F. de Diego, P. Gayán, and J. Celaya, *Mapping of the range of operational conditions for Cu-, Fe-, and Ni-based oxygen carriers in chemical-looping combustion.* Chemical Engineering Science, 2007. **62**(1): p. 533-549.
12. Lyngfelt, A., *Chemical-looping combustion of solid fuels–status of development.* Applied Energy, 2014. **113**: p. 1869-1873.
13. Berguerand, N. and A. Lyngfelt, *The use of petroleum coke as fuel in a 10kWth chemical-looping combustor.* International Journal of Greenhouse Gas Control, 2008. **2**(2): p. 169-179.
14. Adánez, J., L. De Diego, F. García-Labiano, P. Gayán, A. Abad, and J. Palacios, *Selection of oxygen carriers for chemical-looping combustion.* Energy & Fuels, 2004. **18**(2): p. 371-377.
15. Ishida, M. and H. Jin, *A novel chemical-looping combustor without NOx formation.* Industrial & engineering chemistry research, 1996. **35**(7): p. 2469-2472.
16. Abad, A., J. Adánez Elorza, D. Poza, P. Gayán Sanz, F. García Labiano, and A. Lyngfelt, *Fuel reactor model validation: Assessment of the key parameters affecting the chemical-looping combustion of coal.* 2013.
17. Zevenhoven-Onderwater, M., J.-P. Blomquist, B.-J. Skrifvars, R. Backman, and M. Hupa, *The prediction of behaviour of ashes from five different solid fuels in fluidised bed combustion.* Fuel, 2000. **79**(11): p. 1353-1361.
18. Shen, L., J. Wu, and J. Xiao, *Experiments on chemical looping combustion of coal with a NiO based oxygen carrier.* Combustion and Flame, 2009. **156**(3): p. 721-728.

19. Leion, H., T. Mattisson, and A. Lyngfelt, *Solid fuels in chemical-looping combustion.* International Journal of Greenhouse Gas Control, 2008. **2**(2): p. 180-193.
20. *Coal Mining - Quarterly Update 12/16/2013*. 2013, Hoover's Inc.: Austin. p. 0.
21. Schweinfurth, S.P. and R.B. Finkelman, *Coal--a complex natural resource: an overview of factors affecting coal quality and use in the United States*. Vol. 1143. 2003: US Dept. of the Interior, US Geological Survey.
22. Leion, H., T. Mattisson, and A. Lyngfelt, *The use of petroleum coke as fuel in chemical-looping combustion.* Fuel, 2007. **86**(12): p. 1947-1958.
23. Saha, C. and S. Bhattacharya, *Comparison of CuO and NiO as oxygen carrier in chemical looping combustion of a Victorian brown coal.* International Journal of Hydrogen Energy, 2011. **36**(18): p. 12048-12057.
24. Jerndal, E., T. Mattisson, and A. Lyngfelt, *Thermal analysis of chemical-looping combustion.* Chemical Engineering Research and Design, 2006. **84**(9): p. 795-806.
25. Wang, B., R. Yan, H. Zhao, Y. Zheng, Z. Liu, and C. Zheng, *Investigation of chemical looping combustion of coal with CuFe2O4 oxygen carrier.* Energy & Fuels, 2011. **25**(7): p. 3344-3354.
26. Leion, H., E. Jerndal, B.-M. Steenari, S. Hermansson, M. Israelsson, E. Jansson, M. Johnsson, R. Thunberg, A. Vadenbo, T. Mattisson, and A. Lyngfelt, *Solid fuels in chemical-looping combustion using oxide scale and unprocessed iron ore as oxygen carriers.* Fuel, 2009. **88**(10): p. 1945-1954.
27. Linderholm, C., A. Lyngfelt, A. Cuadrat, and E. Jerndal, *Chemical-looping combustion of solid fuels–Operation in a 10kW unit with two fuels, above-bed and in-bed fuel feed and two oxygen carriers, manganese ore and ilmenite.* Fuel, 2012. **102**: p. 808-822.
28. Leion, H., A. Lyngfelt, M. Johansson, E. Jerndal, and T. Mattisson, *The use of ilmenite as an oxygen carrier in chemical-looping combustion.* Chemical Engineering Research and Design, 2008. **86**(9): p. 1017-1026.
29. Cuadrat, A., A. Abad, J. Adánez, L. De Diego, F. García-Labiano, and P. Gayán, *Behavior of ilmenite as oxygen carrier in chemical-looping combustion.* Fuel Processing Technology, 2012. **94**(1): p. 101-112.
30. Berguerand, N. and A. Lyngfelt, *Batch testing of solid fuels with ilmenite in a 10kWth chemical-looping combustor.* Fuel, 2010. **89**(8): p. 1749-1762.
31. Keller, M., M. Arjmand, H. Leion, and T. Mattisson, *Interaction of mineral matter of coal with oxygen carriers in chemical-looping combustion (CLC).* Chemical Engineering Research and Design, 2013.
32. Fan, Y. and R.V. Siriwardane, *Novel New Oxygen Carriers for Chemical Looping Combustion of Solid Fuels.* Energy & Fuels, 2014.
33. Siriwardane, R., H. Tian, T. Simonyi, and J. Poston, *Synergetic effects of mixed copper–iron oxides oxygen carriers in chemical looping combustion.* Fuel, 2013. **108**: p. 319-333.
34. Australian-Government-Geoscience-Australia. *Iron Fact Sheet - Australian atlas of minerals resources, mines & processing centers*. 2014-03-05]; Available from: http://www.australianminesatlas.gov.au/education/fact_sheets/iron.html.
35. Monazam, E.R., R.W. Breault, and R. Siriwardane, *Reduction of hematite (Fe2O3) to wüstite (FeO) by carbon monoxide (CO) for chemical looping combustion.* Chemical Engineering Journal, 2014. **242**: p. 204-210.
36. Magnacca, G., G. Cerrato, C. Morterra, M. Signoretto, F. Somma, and F. Pinna, *Structural and surface characterization of pure and sulfated iron oxides.* Chemistry of materials, 2003. **15**(3): p. 675-687.

37. Li, K., H. Wang, Y. Wei, and D. Yan, *Syngas production from methane and air via a redox process using Ce–Fe mixed oxides as oxygen carriers.* Applied Catalysis B: Environmental, 2010. **97**(3): p. 361-372.
38. Wimmers, O., P. Arnoldy, and J. Moulijn, *Determination of the reduction mechanism by temperature-programmed reduction: application to small iron oxide (Fe2O3) particles.* The Journal of Physical Chemistry, 1986. **90**(7): p. 1331-1337.
39. Mattisson, T., M. Johansson, and A. Lyngfelt, *Multicycle reduction and oxidation of different types of iron oxide particles application to chemical-looping combustion.* Energy & Fuels, 2004. **18**(3): p. 628-637.
40. Tian, H., R. Siriwardane, T. Simonyi, and J. Poston, *Natural Ores as Oxygen Carriers in Chemical Looping Combustion.* Energy & Fuels, 2013. **27**(8): p. 4108-4118.
41. Rubel, A., Y. Zhang, K. Liu, and J. Neathery, *Effect of ash on oxygen carriers for the application of chemical looping combustion to a high carbon char.* Oil & Gas Science and Technology–Revue d'IFP Energies nouvelles, 2011. **66**(2): p. 291-300.
42. Markström, P., C. Linderholm, and A. Lyngfelt, *Operation of a 100kW chemical-looping combustor with Mexican petroleum coke and Cerrejón coal.* Applied Energy, 2014. **113**: p. 1830-1835.
43. Markström, P., A. Lyngfelt, and C. Linderholm. *Chemical-looping combustion in a 100 kW unit for solid fuels*. in *21st International Conference on Fluidized Bed Combustion, June*. 2012.
44. Shen, L., J. Wu, J. Xiao, Q. Song, and R. Xiao, *Chemical-looping combustion of biomass in a 10 kWth reactor with iron oxide as an oxygen carrier.* Energy & Fuels, 2009. **23**(5): p. 2498-2505.
45. Abad, A., I. Adánez-Rubio, P. Gayán, F. García-Labiano, L.F. de Diego, and J. Adánez, *Demonstration of chemical-looping with oxygen uncoupling (CLOU) process in a 1.5 kWth continuously operating unit using a Cu-based oxygen-carrier.* International Journal of Greenhouse Gas Control, 2012. **6**: p. 189-200.
46. Yazdanpanah, M., A. Forret, T. Gauthier, and A. Delebarre, *Modeling of CH4 combustion with NiO/NiAl2O4 in a 10kWth CLC pilot plant.* Applied Energy, 2014. **113**: p. 1933-1944.
47. Thon, A., M. Kramp, E.-U. Hartge, S. Heinrich, and J. Werther, *Operational experience with a system of coupled fluidized beds for chemical looping combustion of solid fuels using ilmenite as oxygen carrier.* Applied Energy, 2013.
48. Orth, M., J. Ströhle, and B. Epple. *Design and Operation of a 1 MWth Chemical Looping Plant*. in *Proc. 2nd Int. Conf. Chemical Looping, Darmstadt, Germany*. 2012.
49. Abdulally, I. and C. Beal. *Alstom's Chemical Looping Prototypes Program Update*. in *Proc. From the 37th Int. Technical Conf. on Clean Coal & Fuel Systems*. 2012.
50. Saha, C. and S. Bhattacharya, *Chemical looping combustion of low-ash and high-ash low rank coals using different metal oxides–A thermogravimetric analyser study.* Fuel, 2012. **97**: p. 137-150.
51. Fan, L., F. Li, and S. Ramkumar, *Utilization of chemical looping strategy in coal gasification processes.* Particuology, 2008. **6**(3): p. 131-142.
52. Liu, B., X.-m. Yang, W.-l. Song, and W.-g. Lin, *Process simulation of formation and emission of NO and N2O during coal decoupling combustion in a circulating fluidized bed combustor using Aspen Plus.* Chemical Engineering Science, 2012. **71**: p. 375-391.
53. Abad, A., F. García-Labiano, L.F. de Diego, P. Gayán, and J. Adánez, *Reduction kinetics of Cu-, Ni-, and Fe-based oxygen carriers using syngas (CO+ H2) for chemical-looping combustion.* Energy & Fuels, 2007. **21**(4): p. 1843-1853.

54. Bohnt, C., J. Cleeton, C. Miiller, S. Scotr, and J. Dennis. *Measuring the kinetics of the reduction of iron oxide with carbon monoxide in a fluidized bed*. in *Proceedings of the 20th International Conference on Fluidized Bed Combustion*. 2010. Springer.
55. Son, S.R. and S.D. Kim, *Chemical-looping combustion with NiO and Fe2O3 in a thermobalance and circulating fluidized bed reactor with double loops.* Industrial & engineering chemistry research, 2006. **45**(8): p. 2689-2696.
56. Ye, D., J.B. Agnew, and D. Zhang, *Gasification of a South Australian low-rank coal with carbon dioxide and steam: kinetics and reactivity studies.* Fuel, 1998. **77**(11): p. 1209-1219.
57. Gu, J., S. Wu, X. Zhang, Y. Wu, and J. Gao, *CO2-gasification reactivity of different carbonaceous materials at elevated temperatures.* Energy Sources, Part A, 2009. **31**(3): p. 232-243.
58. Osafune, K. and H. Marsh, *Gasification kinetics of coal chars in carbon dioxide.* Fuel, 1988. **67**(3): p. 384-388.
59. Kovacik, G., A. Chambers, and B. Özüm, *CO2 gasification kinetics of two Alberta coal chars.* The Canadian Journal of chemical engineering, 1991. **69**(3): p. 811-815.
60. Zhang, S., S. Rajendran, R. Xiao, and S. Bhattacharya, *Chemical-Looping Combustion of Victorian Brown Coal Using Mixed Oxygen Carriers of Iron and Manganese Oxides*, in *CHEMECA*. 2013: Brisbane Convention & Exhibition Centre.
61. Roberts, D. and D. Harris, *Char gasification with O2, CO2, and H2O: Effects of pressure on intrinsic reaction kinetics.* Energy & Fuels, 2000. **14**(2): p. 483-489.
62. Garcia-Labiano, F., J. Adanez, L.F. de Diego, P. Gayán, and A. Abad, *Effect of pressure on the behavior of copper-, iron-, and nickel-based oxygen carriers for chemical-looping combustion.* Energy & Fuels, 2006. **20**(1): p. 26-33.

# APPENDIX

## TPR Measurements of oxygen carriers in cycle 2 to 5

The reduction cycles are here presented for each oxygen carrier.

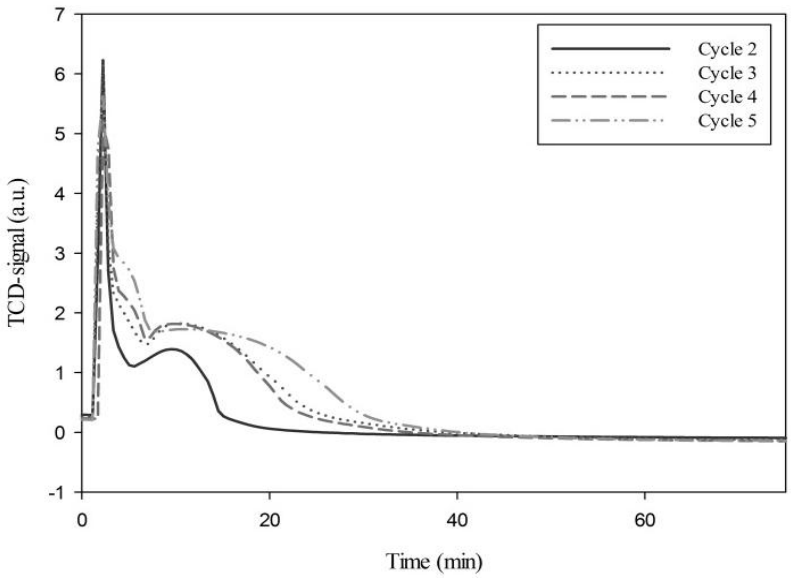


**Figure 25. TPR measurements of cycle 2-5 of WA-1**

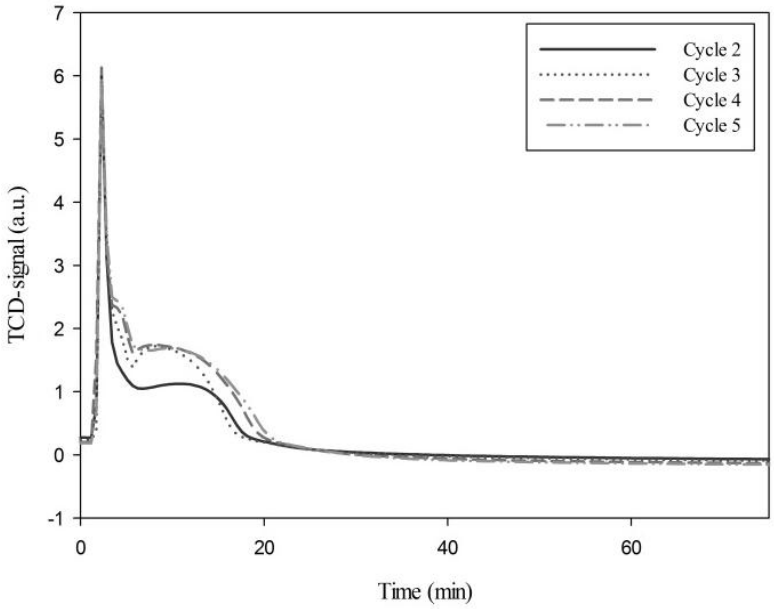


**Figure 26.TPR measurements of cycle 2-5 of WA-2**

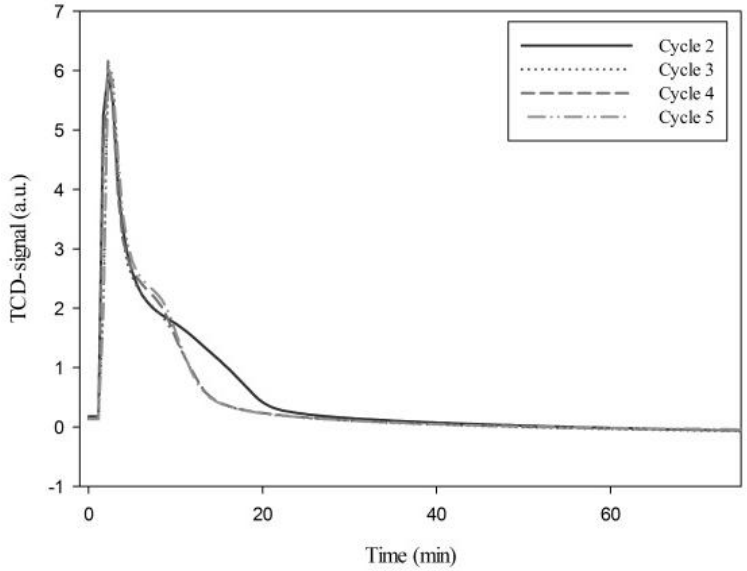


**Figure 27. TPR measurements of cycle 2-5 of Limonite**

## SEM-figures fresh and used sample from TGA

Here are SEM pictures of WA-1, WA-2, Limonite and Calcined WA-1, both fresh samples and samples used in the TGA, with $CO_2$ and steam

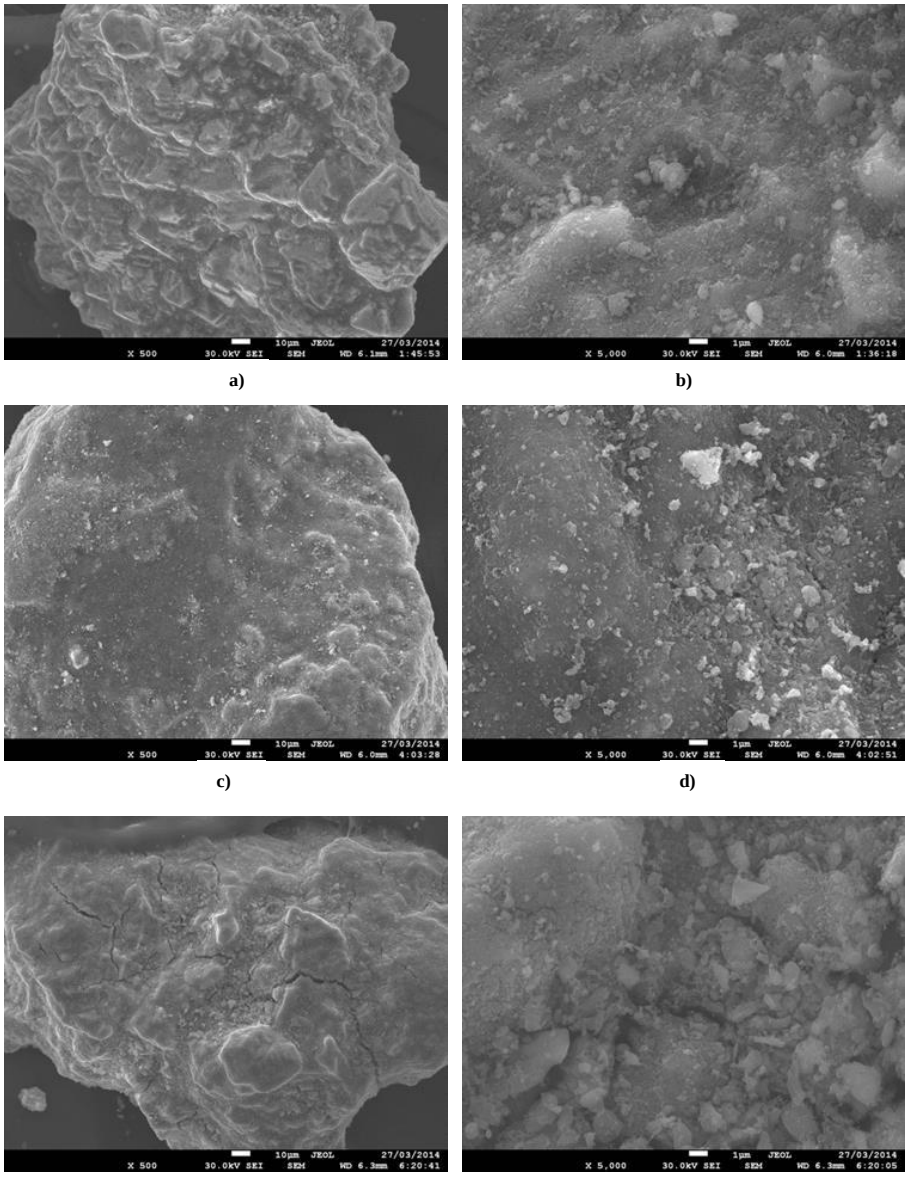


**Figure 28. SEM pictures of WA-1. a) Fresh 500x, b) Fresh 5000x, c) 5 cycles in CO2 500x, d) 5 cycles in CO2 5000x, e) 2 cycles in steam 500x, f) 5 cycles in steam 5000x**

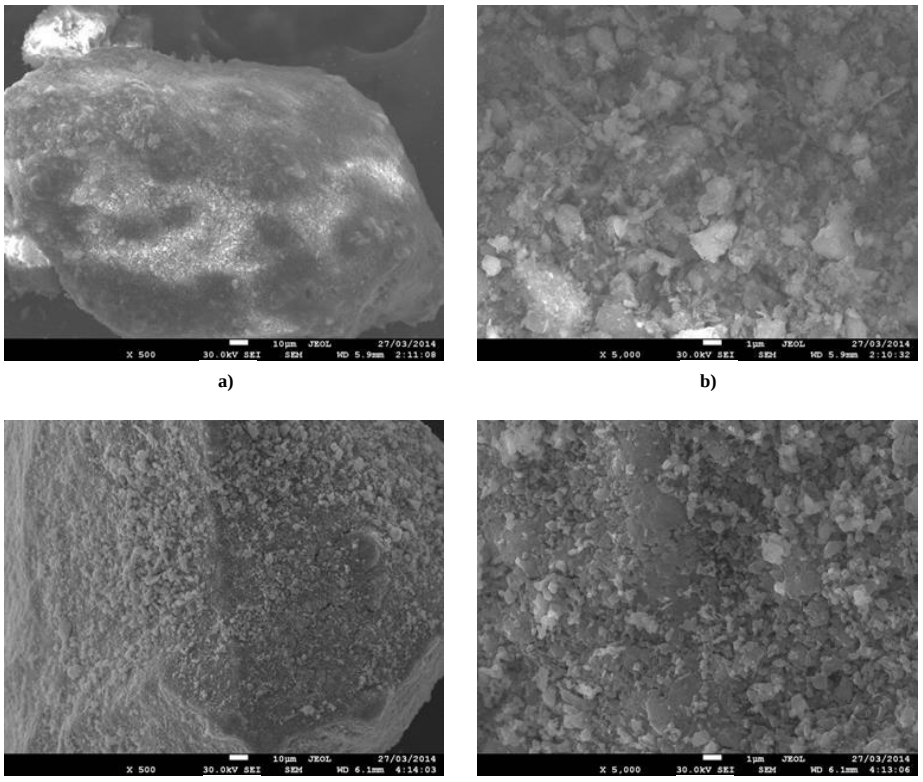


a) b)

c) d)

**Figure 29. SEM pictures of WA-2. a) Fresh 500x, b) Fresh 5000x, c) 5 cycles in CO2 500x, d) 5 cycles in CO2 5000x**

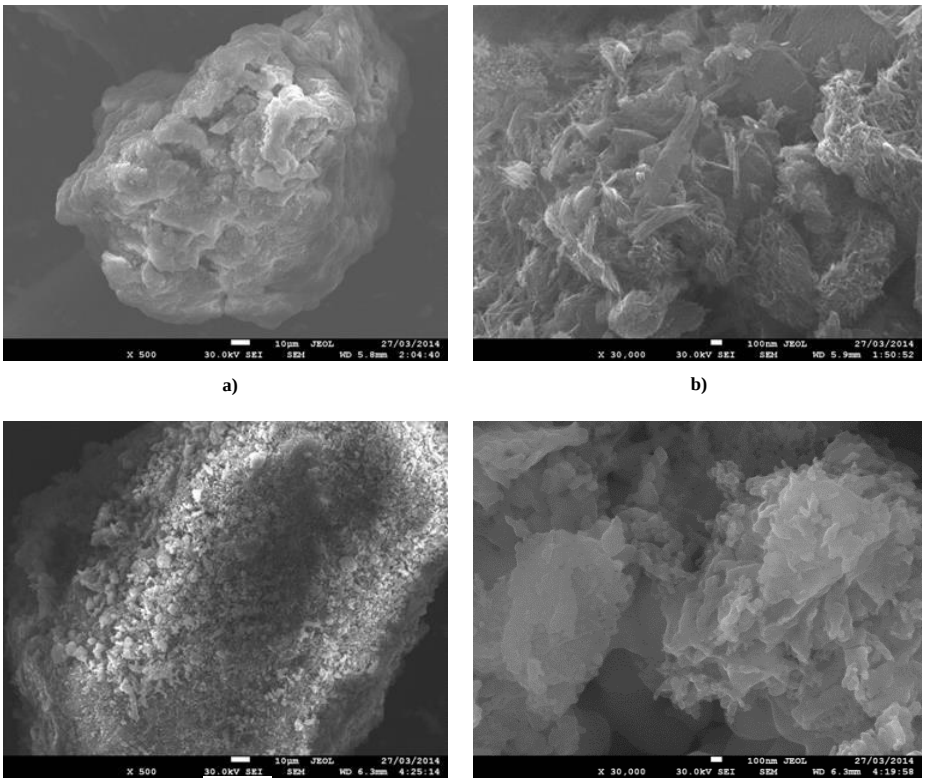


a) b)

c) d)

**Figure 30. SEM pictures of Limonite. a) Fresh 500x, b) Fresh 30 000x, c) 5 cycles in CO2 500x, d) 5 cycles in CO2 30 000x**

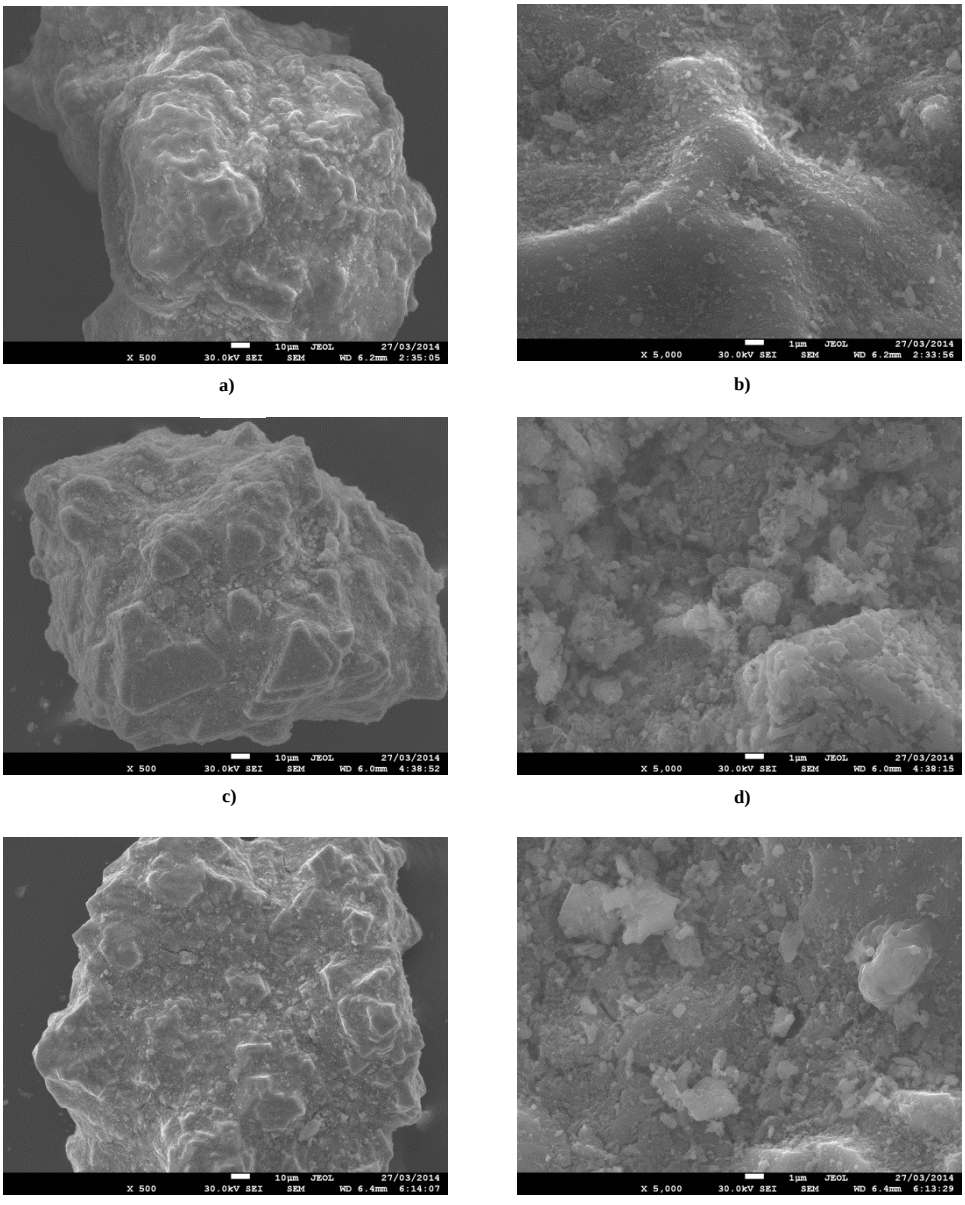


**a)** **b)** **c)** **d)** **e)** **f)**

**Figure 31. SEM pictures of Calcined WA-1. a) Calcined 500x, b) Calcined 5000x, c) 5 cycles in CO2 500x, d) 5 cycles in CO2 5000x, e) 2 cycles in steam 500x, f) 5 cycles in steam 5000x**

## EDX-figures for WA-1 fresh and Calcined sample

The EDX measurements of the fresh WA-1 and the Calcined WA-1.Displaying the unused sample, the sample used for 5 runs in $CO_2$ gasification and 2 runs in steam gasification, in the TGA

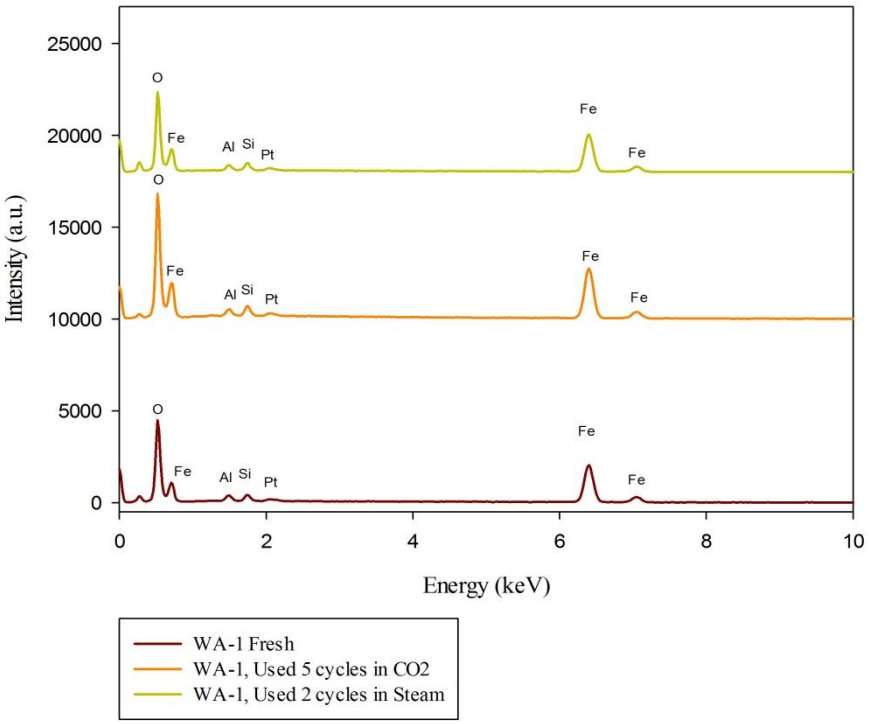


**Figure 32. Samples of Fresh WA-1,WA-1 used both in CO2 and Steam in TGA**

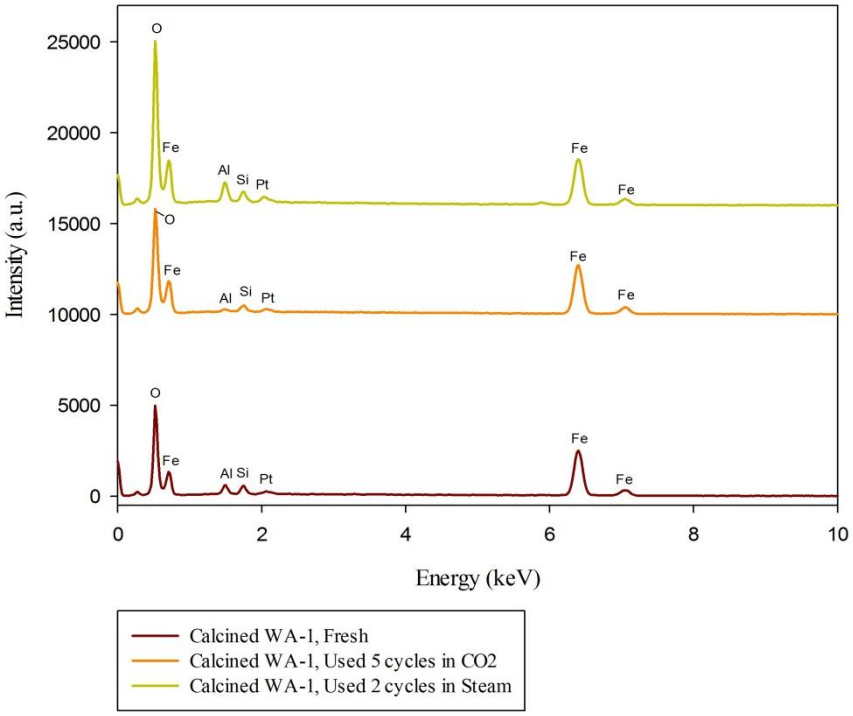


**Figure 33. Samples of Calcined WA-1, Calcined WA-1 used both in CO2 and Steam in TGA**

## SEM figures from the Fluidized bed reactor

Here are SEM pictures of WA-1, WA-2 and Limonite, both fresh samples and samples used in the fluidized bedreactor.

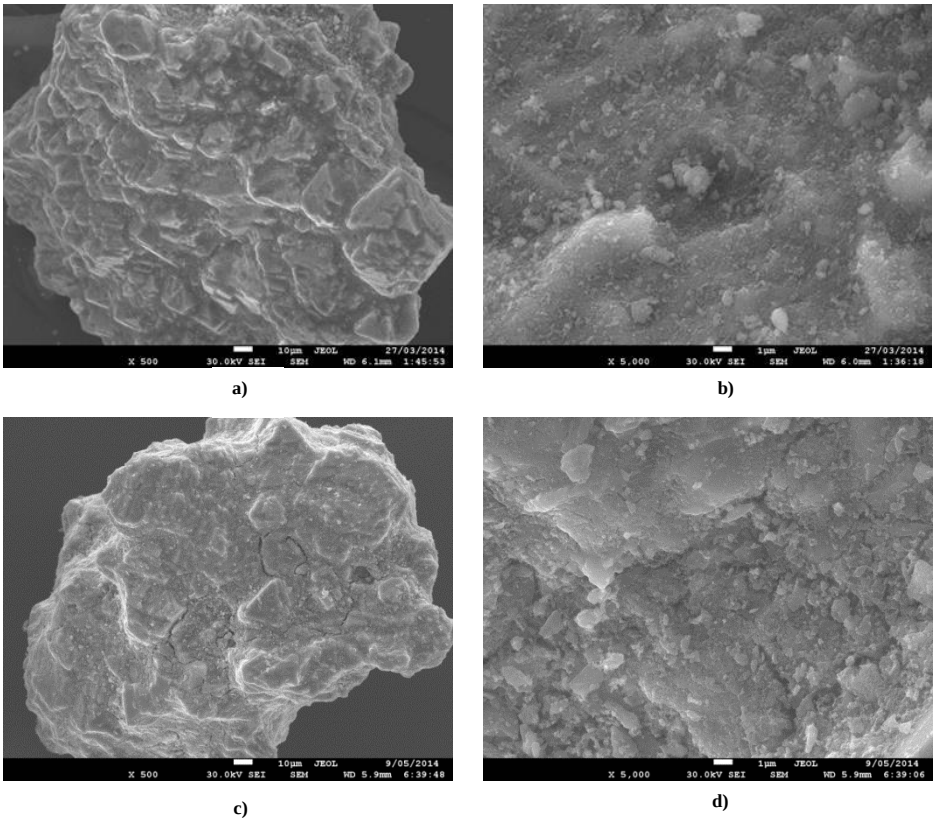


**a)** **b)**

**c)** **d)**

**Figure 34. SEM pictures of WA-1. a) Fresh 500x, b) Fresh 5000x, c) 10 cycles, 500x, d) 10 cycles, 5000x,**

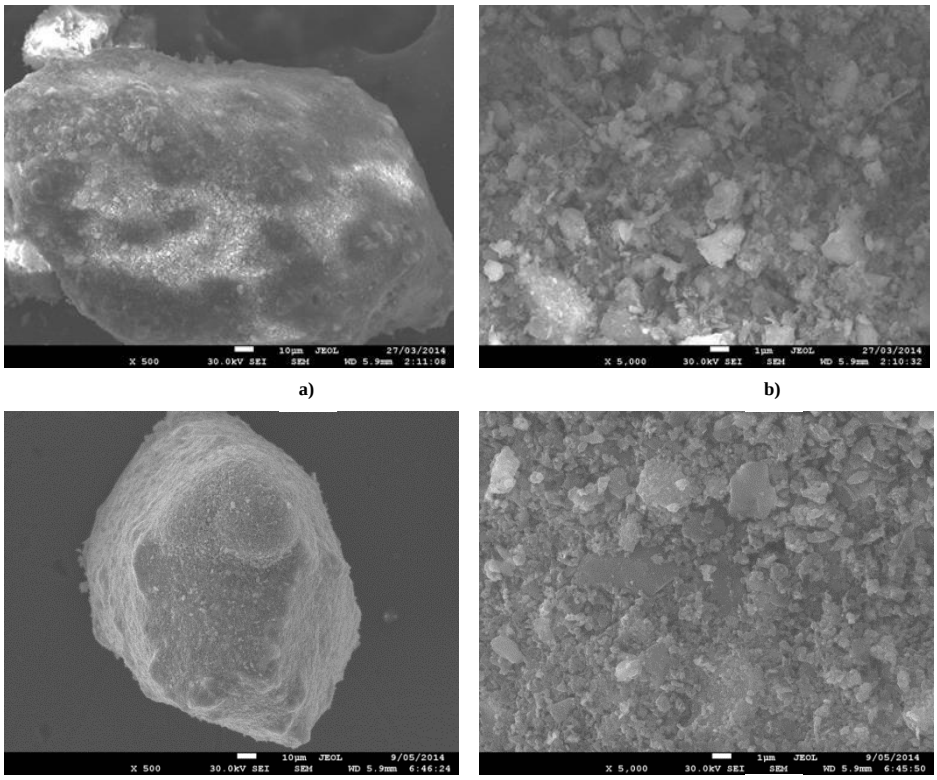


**a)** **b)**

**c)** **d)**

**Figure 35. SEM pictures of WA-2. a) Fresh 500x, b) Fresh 5000x, c) 10 cycles, 500x, d) 10 cycles, 5000x**

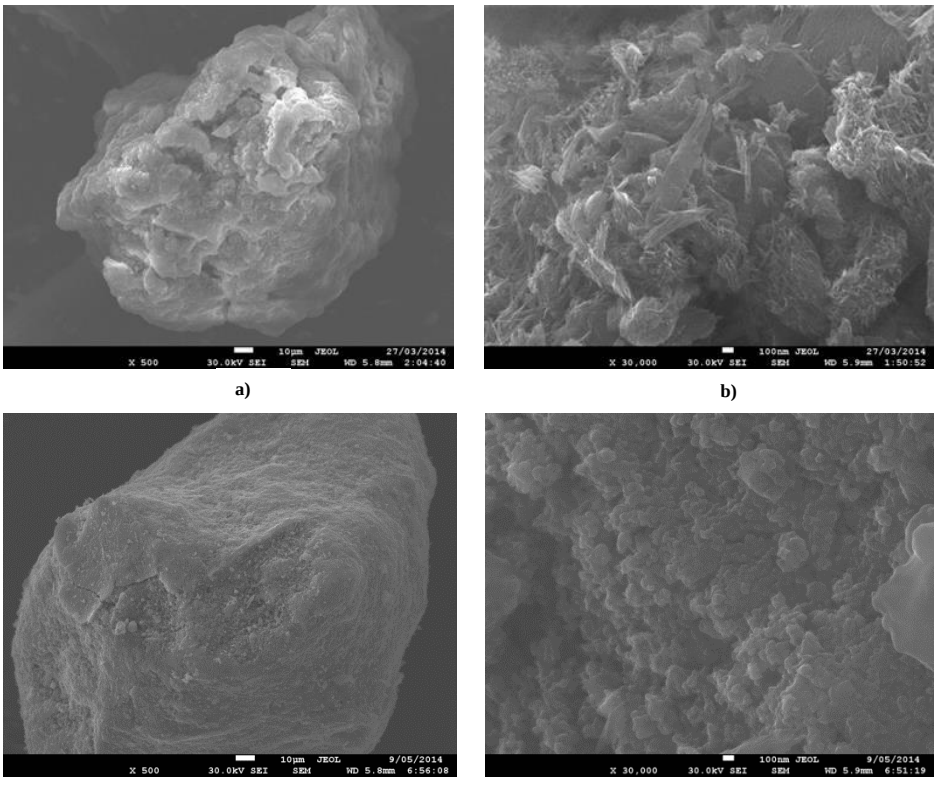


**a)** **b)**

**c)** **d)**

**Figure 36. SEM pictures of Limonite. a) Fresh 500x, b) Fresh 30 000x, c) 10 cycles, 500x, d) 10 cycles 30 000x**

**Model figuration of the Aspen modeling**

**Red ring** is Fuel reactor and **Blue ring** is Air reactor

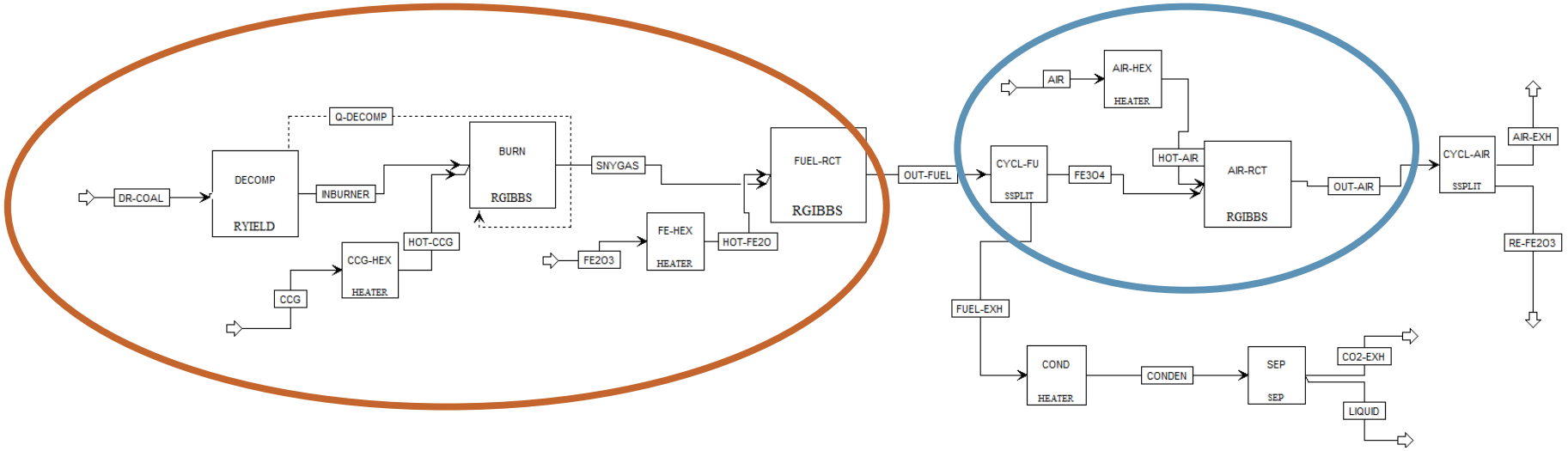


**Figure 37. Aspen plus model with RGibbs reactors**

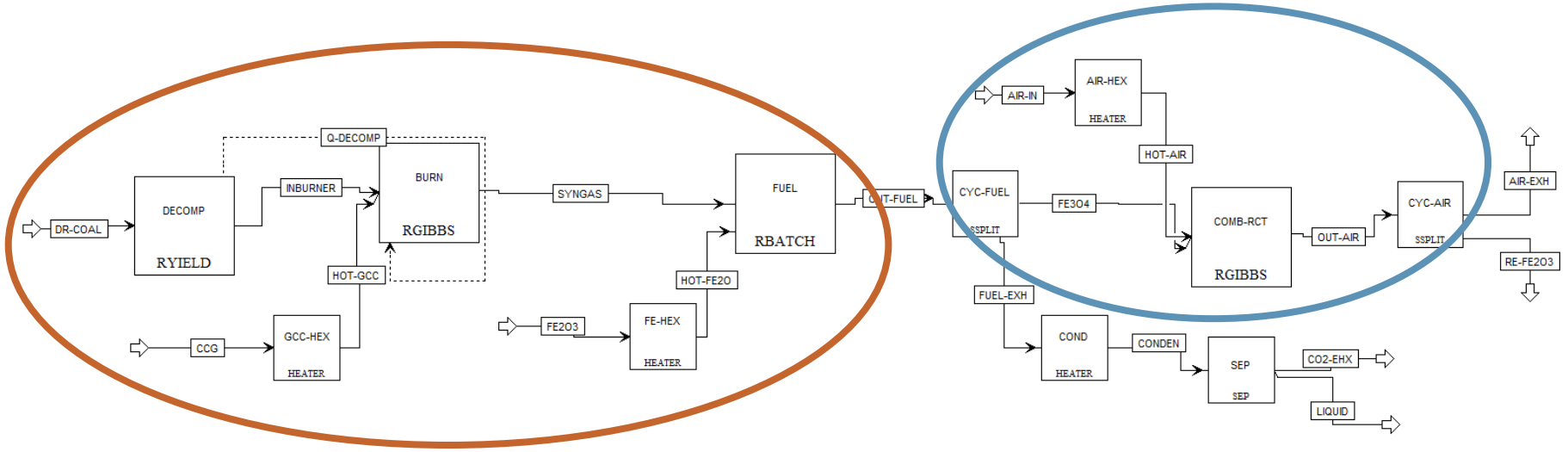


**Figure 38. Aspen plus model with one RBatch reactor for fuel reactor used when evaluating reduction kinetics**

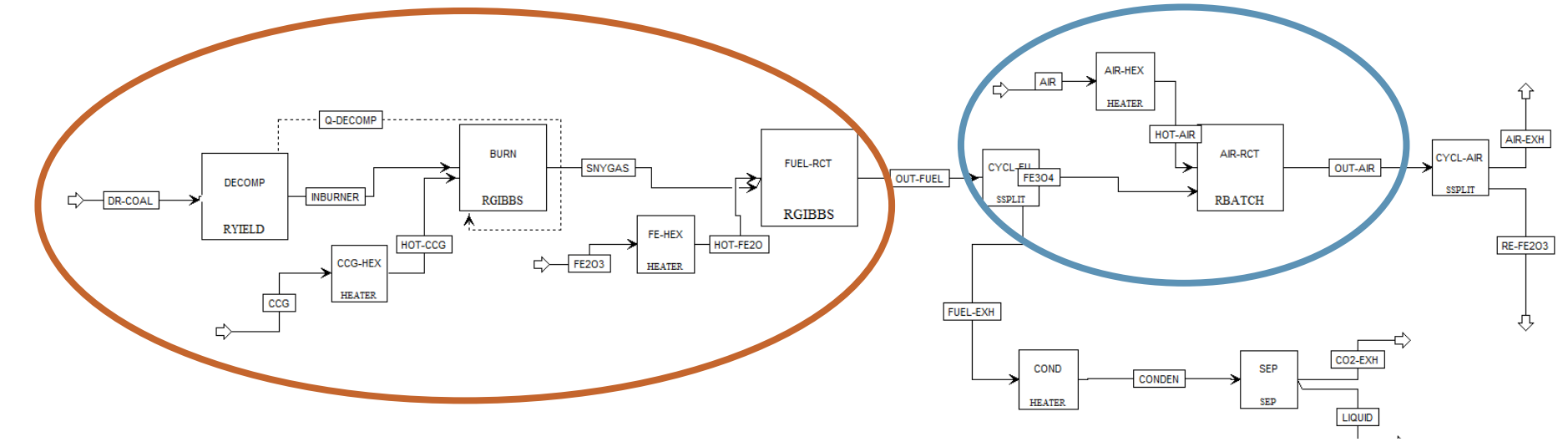


**Figure 39. Aspen plus model with one RBatch reactor for air reactor used when evaluated oxidation kinetics**

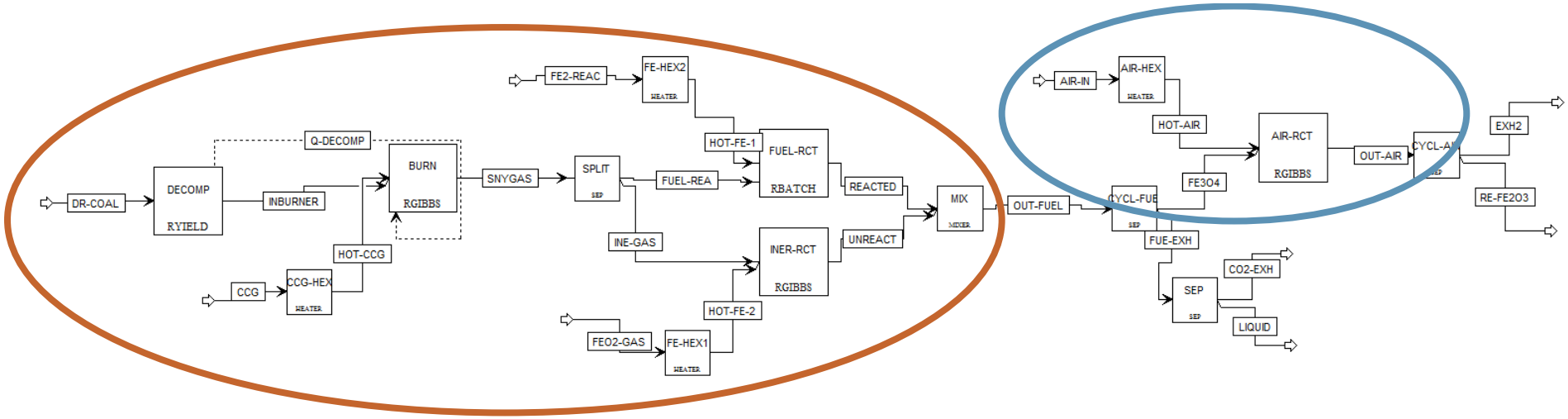


**Figure 40. Aspen plus model with one RBatch reactor and one RGibbs reactor modelling the reduction reactor and effects of other possible reactions**

## Conversion of species when using Gibbs reactor

The conversion over the fuel reactor, when change in temperature both in the fuel reactor and in the decomposing reactor is here presented:

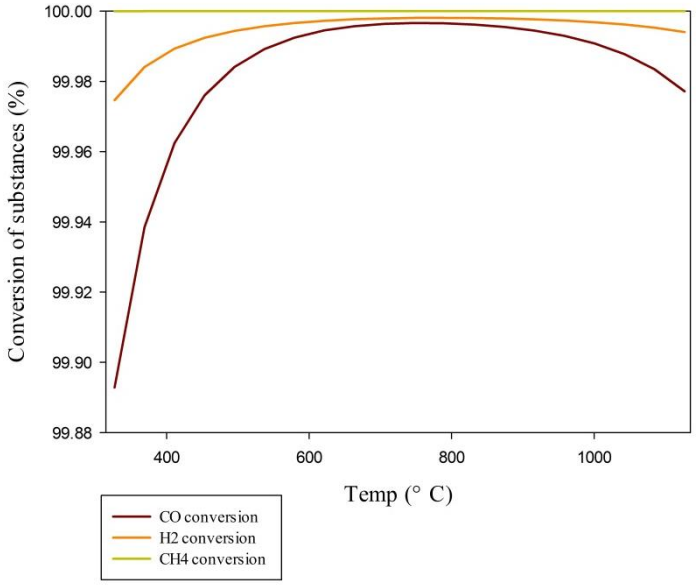


**Figure 41. Conversion of species in fuel reactor, when changing temperature in both fuel and decomposing reactor**

## Sensitivity analysis on temperature dependence for different kinetics

Three different kinetics are used for following analysis on the fuel reactor

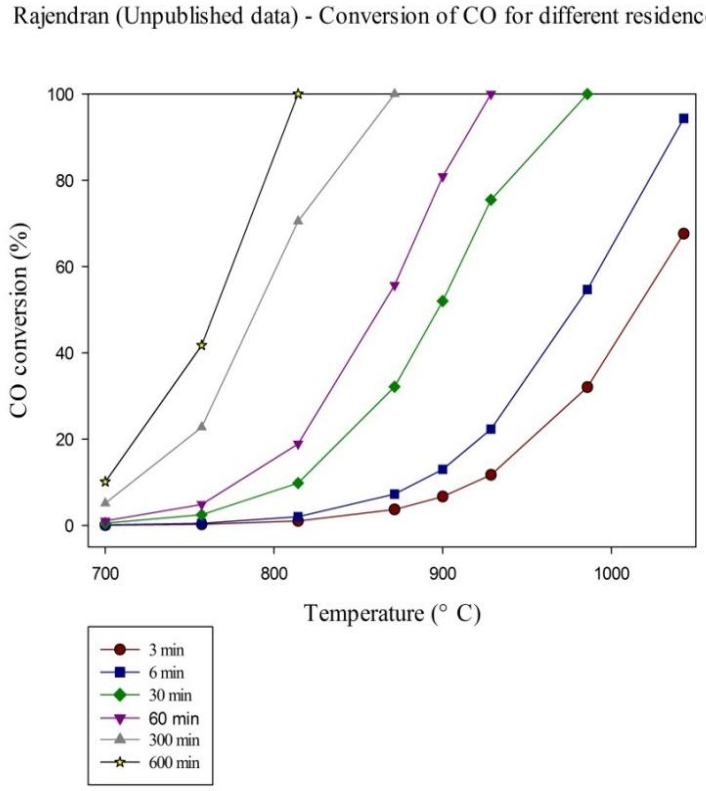


**Figure 42. CO conversion depending on the residence time and temperature for kinetics by Rajendran**

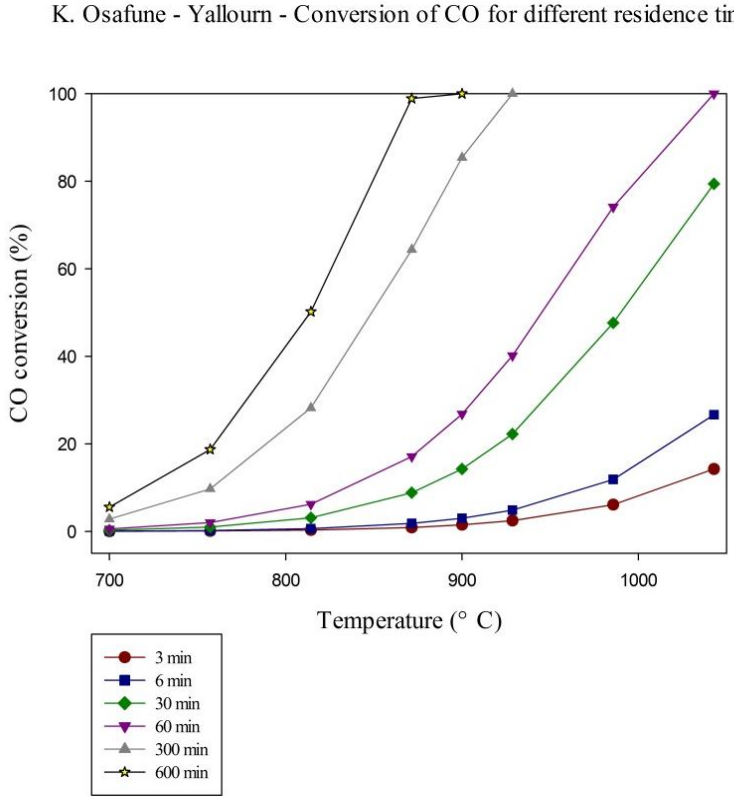


**Figure 43. CO conversion depending on the residence time and temperature for kinetics by Osafune et al. (1988)**

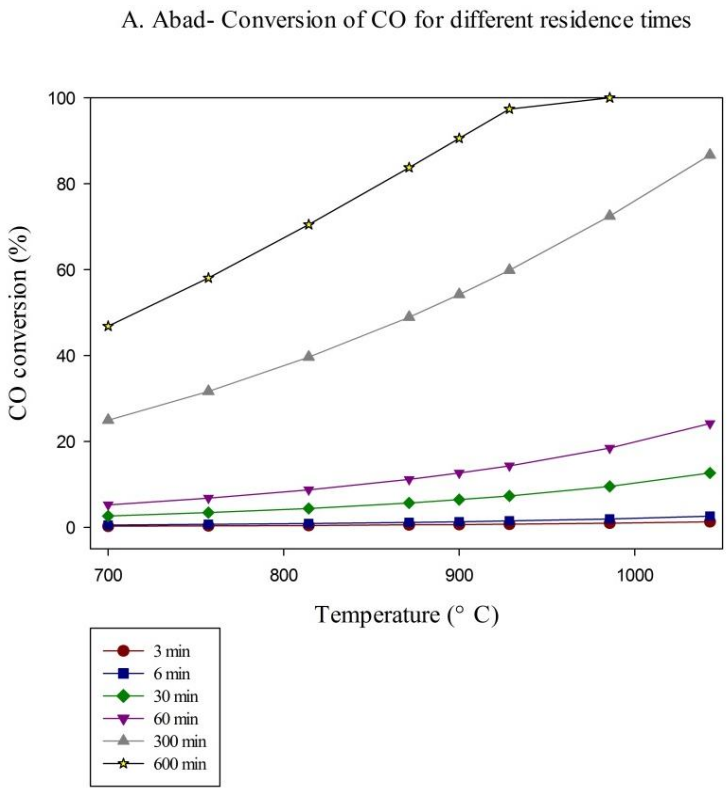


**Figure 44. CO conversion depending on the residence time and temperature for kinetics by Abad et al. (2007)**

Two different kinetics are used for following analysis on air reactor.

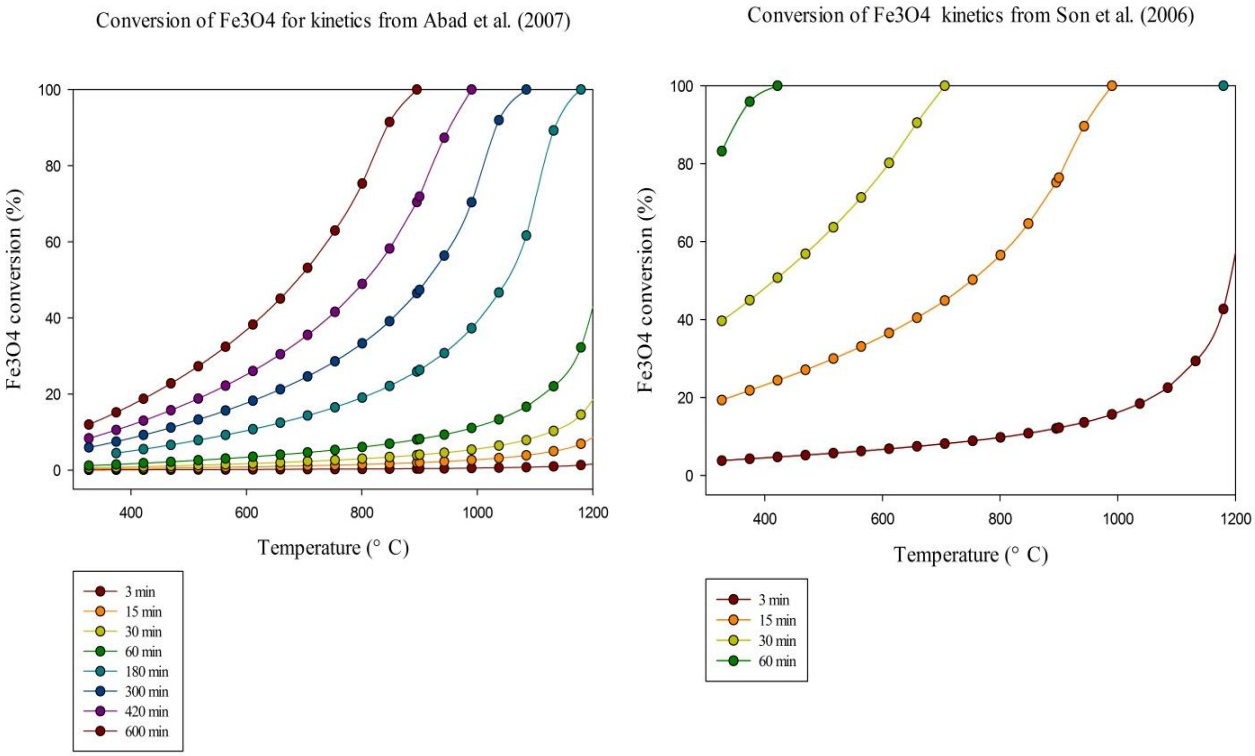


**Figure 45. $Fe_3O_4$ conversion with two different oxidation kinetics**